Some aspects of tensile fracture behaviour and structural response of cementitious materials

Zhou, Fan Ping

1988

DIVISION OF BUILDING MATERIALS
LUND INSTITUTE OF TECHNOLOGY

Some aspects of
TENSILE FRACTURE BEHAVIOUR
and STRUCTURAL RESPONSE
of CEMENTITIOUS MATERIALS

FANPING ZHOU

REPORT TVBM-1008
LUND - SWEDEN 1988

CODEN: LUTVDG/(TVBM-1008)/1-76/(1988)

Some aspects of
TENSILE FRACTURE BEHAVIOUR
and STRUCTURAL RESPONSE
of CEMENTITIOUS MATERIALS

FANPING ZHOU

ISSN 0348-7911

THE SECOND, REVISED EDITION

ACKNOWLEDGEMENTS

The work presented in this report has been carried out at the Division of Building Materials, Lund Institute of Technology, Sweden.

First of all I wish to express my deepest gratitude to my supervisor, Professor Arne Hillerborg for his invaluable guidance, support and encouragement, as well as for reading the manuscript and proposing improvements. I would like to thank Tech. Dr. Per-Johan Gustafsson, at the Division of Structural Mechanics, for the inspiring discussions.

Sincere thanks are directed to Civ. Eng. Manouchehr Hassanzadeh and Technician Bosse Johansson for their never-ending patience and skillful assistance in the experimental work. I am also indebted to Technicians Ingemar Larsson, Sture Sahlén, Stefan Backe and Bengt Linné for solving experimental problems.

Mrs Britt Andersson has prepared all the drawings with her great skill and patience. Miss Monica Hedin has corrected linguistic errors in a highly accurate way. I am deeply grateful for their efficient 'gold-plating' work. I would like to thank Mr. Olof Peterson for his kindness and help in preparing the front cover.

Last but not least I would like to thank all other members of the staff at the Division for their support and co-operation which have made this work possible.

Lund, December 1988

Fanping Zhou

ABSTRACT

This report deals with stability and validity analyses of direct tension tests, and an investigation into structural behaviour of various materials in tensile fracture.

The influence of rotation in damage zone on the stress-deformation curve is investigated. The role of rotation stiffness of testing set-ups for a stable tension test is analysed. The bump effect, i.e. steep stress drops in stress-deformation curves, is studied. The theoretical analyses agree with experimental observations.

A number of tests, with both statically determinate and indeterminate specimens, are performed to investigate tensile fracture behaviour of various materials, from brittle to tough. Compared to the experimental results, the FCM model seems able to yield proper predictions.

CONTENTS

1 INTRODUCTION

1.1 General

In structural engineering concrete materials are assigned to take mainly compressive stresses, while reinforcements carry tensile stresses. Although tensile cracking is usually the major contributor to the nonlinear behaviour of reinforced concrete structures. Furthermore, it can impose great influence even on ultimate load bearing capacity in some cases.

The tensile failure of concrete is generally regarded as brittle. The fracture process is characterized by gradual separation of discrete cracks. No slip or yielding behaviour occurs.

Concrete materials are usually treated simply as elastic-brittle ones. The strength in the tension-loading direction is assumed to abruptly go to zero after a crack has formed. Such an approach was incorporated into finite element analysis of reinforced concrete structures by Ngo and Scordelis (32), when the tensile cracking was taken into account for the first time. This approach can be expected to predict the lower bound of strength of a concrete structure.

A lot of work has been done in order to apply linear elastic fracture mechanics (LEFM) to plain concrete since 1961 (28). But LEFM does not seem to be directly applicable to concrete structures of laboratory size due to the stable, large fracture process zone in front of the crack-tip.

Based on analysis of tensile fracture behaviour, a more realistic model, the so-called Fictitious Crack Model (FCM), was put forward

by Hillerborg, Modéer and Petersson (19). It has been successfully applied to analyse tensile fracture behaviour of concrete and similar materials.

1.2 Aim and scope of the report

The uniaxial stress-deformation σ-w curve, forming the basis for the FCM model and some other fracture models, is very important material input for studies of tensile fracture behaviour. Unfortunately, many experimental results from direct tension tests show that structural behaviour remarkably distorts the real material property. One of the objectives in this report is to perform stability and validity analyses of direct tension tests, and to investigate how to obtain reliable tests.

Another one is to theoretically and experimentally investigate tensile fracture behaviour of various materials with both statically determinate and indeterminate specimens, and gain some insight into the general applicability of the Fictitious Crack Model.

1.3 Limitations

Some major limitations in analyses of the report are listed as follows:

a) Materials are assumed to be homogenous and isotropic. The smallest dimensions of specimens are chosen to be at least three or four times greater than the largest aggregate or fibre so that the assumption can be reasonably fulfilled.

b) Plane stress state is adopted throughout the analyses in this report.

c) The analyses and tests mainly concentrate on statical or quasi-statical studies.

d) Neither initial stress nor time-dependent effects have been taken into account.

e) Only tensile stress induced fracture is concerned and propagation paths are assumed to be known in advance.

1.4 Outline of contents

Chapter 2 gives a brief description of the Fictitious Crack Model. The basic fracture parameters for the model and determinating methods are reviewed.

Chapter 3 concerns some aspects of finite element calculations used in FCM analysis. Numerical realization of FCM analysis and choice of element type are briefly discussed.

Chapter 4 presents stability and validity analyses of direct tension tests. The influences of notch sensitivity, eccentricity and rotation in damage zone on stress-deformation σ-w curves are investigated. The role of rotation stiffness and material property on a stable and reliable test is analysed.

Chapter 5 presents some investigation into structural behaviour of various materials in three-point bending and frame tests. Comparisons between the experimental results and theoretical predictions are made.

Chapter 6 gives the concluding remarks.

2 FICTITIOUS CRACK MODEL

2.1 Introduction

In recent decades the important contribution of softening behaviour to nonlinear global responses of reinforced concrete structures has been recognized. Thus, main attempts have been made to determine the uniaxial stress-strain law for concrete and similar materials. But a general stress-strain relation is not possible to obtain.

As shown in Fig 2.1, in the pre-peak stage the deformation is uniformly distributed along the whole specimen. But in the post-peak stage, the deformation is so highly localized into the damage zone that it is impossible to find a valid stress-strain

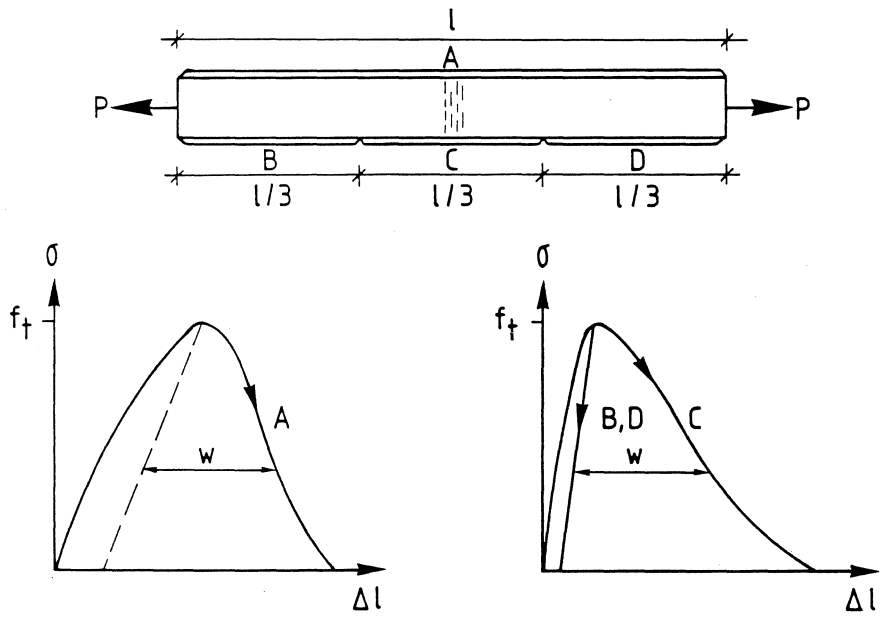

Fig 2.1 Stress-deformation curves dependent on measuring position and gauge lengths in a tensile test. (Hillerborg, 20)

relation. Therefore, the whole deformation history should be described by two relations: a stress-strain σ-ϵ curve for the pre-peak stage and a stress-deformation σ-w curve for the post-peak stage. Based on the analysis of tensile behaviour, the Fictitious Crack Model was proposed by Hillerborg, Modéer and Petersson (19).

2.2 Description of the model

The model is essentially based on a macroscopic modelling of deformation history in the damage zone in uniaxial tension. Some basic assumptions may be made as follows:

(1) Effects of lateral stresses or strains should be negligible.

(2) The fracture energy should mainly be consumed to separate the crack, while the energy dissipation due to accompanied volume change should be comparably small.

According to the model, the whole deformation history of a non-yielding material can be described in the following three stages (Fig 2.2):

(a) Undamaged stage. The material behaviour is governed by the stress-strain relation and can be analysed by continuum mechanics.

Strength Criterion: As soon as the maximum principal stress has reached the tensile strength, a localized damaged zone or a fictitious crack forms perpendicular to the direction of the stress.

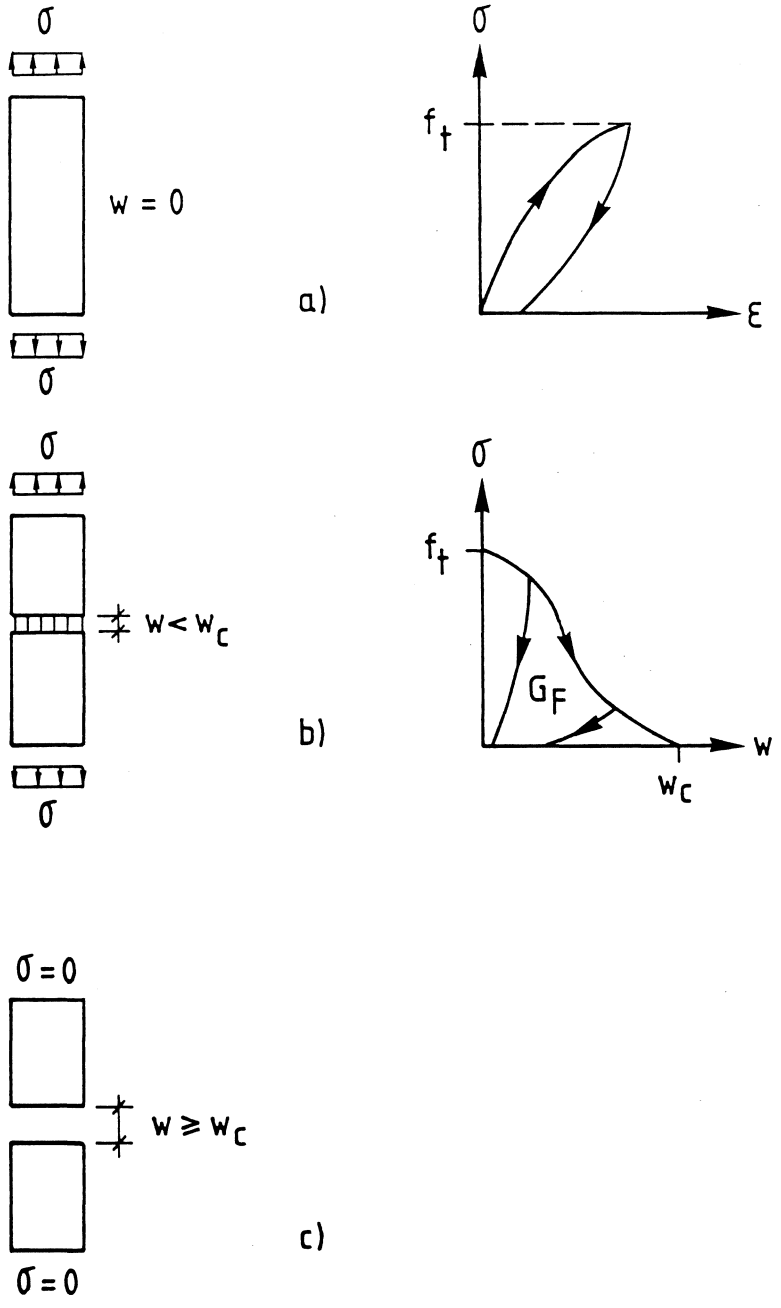

Fig 2.2 Three stages of deformation history
(a) undamaged stage;
(b) strain-localized stage;
(c) separation stage.

(b) Strain-localized stage. As the opening of the damaged zone increases to w_c, the transferred stress of the zone decreases to zero according to the stress-separation relation (σ-w).

Energy Criterion: As soon as fracture energy (G_F) according to the stress-deformation curve has been consumed in the zone, a real crack forms.

(c) Separation stage. The damaged zone is totally separated and no tensile stress can be transferred.

2.3 Material parameters and determination

In practical applications it may be very cumbersome to employ the real σ-ϵ and σ-w curves as material parameters. Some reasonable simplifications have to be made for the convenience of numerical and theoretical analyses.

The stress-strain curve is usually assumed to be linear. It is reasonable for concrete materials, even for fibre concrete in low fiber content. The stress-deformation curve (σ-w) can be approximated as a linear or bilinear one.

The tensile strength f_t, fracture energy G_F and dynamic Young's modulus E are often chosen as material parameters of the FCM model. For the assumed shapes of the two curves, those three parameters can uniquely determine the two curves.

Another combined material parameter is the characteristic length l_{ch} as

$$l_{ch} = EG_F/f_t^2$$

It has a similar form to $(K_c/\sigma_y)^2$ in conventional fracture mechanics, where K_c is fracture toughness and σ_y yielding strength. In a sense, it may be regarded as a measure of the damage zone.

It is worthwhile to mention that the shape of σ-w curve also has notable effects, especially the initial slope (7, 30).

In order to accurately determine the stress-strain curve and the stress-deformation curve, a stable direct tension test should be performed.

For concrete and similar materials the shapes of the stress-strain and stress-deformation curves are well known. Thus, the curves can be indirectly obtained by determination of tensile strength f_t, fracture energy G_F and dynamic Young's modulus E.

A test set-up, proposed by Petersson (36), may be used to determine tensile strength f_t. The modulus E may be determined according to the resonance frequence method (41).

The fracture energy G_F can be determined with a three-point bending test of a notch beam (Fig 2.3), according to the RILEM recommendation (1). The calculation formula is given by

$$G_F = (A1+Mgd)/b(h-a)$$

where M is mass and g the gravitation constant, the other notations are illustrated in Fig 2.3.

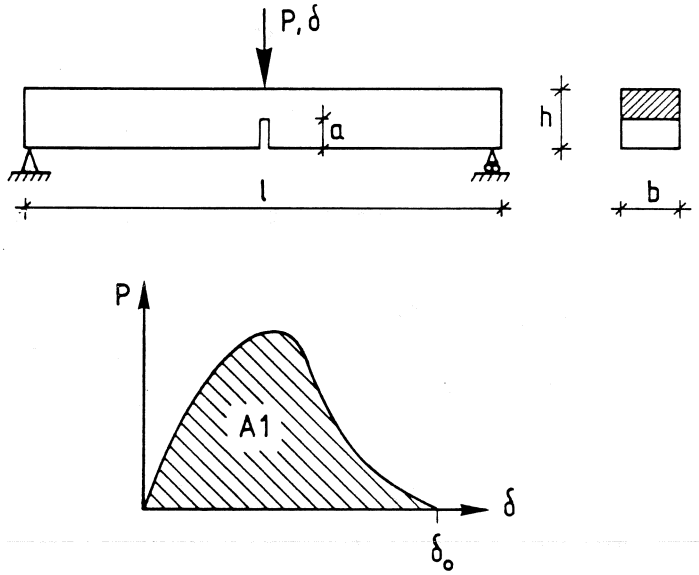

Fig 2.3 RILEM recommendation on determination of fracture energy G_F.

2.4 Main features and applications

The FCM model introduces a strength criterion for crack initiation and a fracture energy criterion for complete development of a real crack. Compared with classical fracture mechanics, the FCM model can be employed to study not only the onset of instability of structures with initial cracks, but also the whole deformation history of structures without pre-crack: from formation and propagation of cracks to complete fracture. Initial stresses, for instance shrinkage stress can be easily treated. Thus, it is possible to analyse real structures by the model.

The model can be used to analyse some basic fracture mechanics problems, for example, notch sensitivity and size dependence of K_c, G_c. It is quite easy and inexpensive to theoretically evaluate test methods used to determining fracture parameters.

In practical applications the model has been employed to study bending problems of beams(37), and bending and crushing failure of pipes of plain concrete (15, 16). Some attempts have also been made to analyse shear failure of reinforced concrete and wooden beams (16). The theoretical studies can properly predict structural behaviour, for instance, size effect, ratio between flexural strength and tensile strength.

3 SOME ASPECTS OF FEM CALCULATIONS

3.1 Introduction

Only in very few cases, it is possible to find an analytical solution for FCM model (11). In practice, however, numerical methods have to be used in FCM analysis.

The finite element method, as the most flexible and general method, naturally becomes the first choice. Some other methods, for instance the boundary element method, have also been used in fracture analysis.

Because of the elimination of stress singularity in the FCM model, no special element type or very fine mesh is necessary. Generally, commercial FEM programs can be used. Of course a small special-purpose program will make FCM analysis more economic and efficient. Such a program has been used in all analyses of the report.

Regarding numerical modelling of damage zones and fracture processes in concrete and similar materials, two methods, the discrete approach and smeared approach, are frequently used. In the report only the discrete approach is employed.

In this chapter the basic technique concerning how to realize the FCM analysis with FEM is described. The choice of element type is briefly discussed.

3.2 Principle of calculations

3.2.1 Material laws and crack propagation path

Basic material laws in FCM analysis are the stress-strain σ-ϵ relation and stress-deformation σ-w relation. In all calculations of the report the stress-strain curve is approximated with a straight line, while the stress-deformation curve is assumed to be step-wise linear.

According to FCM, the direction of crack propagation should be perpendicular to the maximum principal stress. Usually the crack propagation path can be predicted in advance. In such a case the path can be chosen to coincide with interelement boundary. Then only topology updating is required. In all analyses of this report such an approach has been used. If the crack propagation path is not known in advance, both topology and mesh updating are required.

3.2.2 Modelling of damage zone

Damage zone can be modelled by means of springs with negative stiffnesses. Usually if the average stress around a node reaches the uniaxial tensile strength, the node is splitted into two nodes and a negative spring is inserted between them. The stress-deformation relation of the spring is governed by the σ-w curve. If the deformation of the spring reaches the critical opening w_c, the two nodes are completely disconnected. In this way the formation and propagation of a crack can be simulated by means of FEM.

3.2.3 Numerical technique

In solving nonlinear structural problems two basic numerical solution approaches are frequently used. One approach is to choose small load or displacement increments and solve incremental equilibrium equations

$$\{K_T\}(\delta U) = (\delta P)$$

Another approach is to perform the total equilibrium of system equations

$$\{K\}(U) = (P)$$

where $\{K_T\}$ and $\{K\}$ are the tangential and total stiffness matrices, respectively, U is the total displacement and P is the total load.

The former approach is often used where material nonlinearity problems are concerned. The approach is based on the incremental equilibrium, the total equilibrium may not be fulfilled. Small errors in each step can be accumulated and may result in a great drift from the real global response. Certainly, equilibrium iterations in each step can reduce such a drift. But around an extremum point where the tangential stiffness is nearly zero, the equilibrium iteration technique may fail. Thus, the overall response around an extremum point can not be properly predicted unless some special measures have been taken.

In FCM analysis a slightly different approach has been used. The nonlinear global behaviour is modelled by step-wise changing material properties in damage zones.

In each step the smallest load increment which results in change of material property at some point in the damage zone is chosen so that the stiffness matrix remains constant until the next change of material property in some point. Then the corresponding term of the stiffness matrix will be updated and the calculation will be carried out with a new load increment and so on. If the number of nodes in a damage zone is n and the σ-w curve is linearized into m pieces, the total number of calculation steps will be at least $n(m+1)$.

Because the stiffness matrix is constant in each step, no equilibrium iteration is required. The equilibrium equations can be solved exactly, provided that the absolute value of the determinate of the stiffness matrix is not too small. Since the stiffness is updated in a step-wise way, the probability of nearly zero stiffness seems very small. In addition, according to the past experience of FCM analyses such difficulty has never been encountered.

This approach is simple and stable, no complicated solution algorithm is required. It seems able to properly reproduce the nonlinear global response due to tensile fracture.

3.3 Calculation procedure and program

The main procedure in each load step includes linear FEM calculation, determination of load increment and evaluation of stresses, load and displacement, as well as updating of input to the next step.

The load increment may be difficult to determine in some cases, because the nodes in the damage zone can load or unload so that two possible load paths can be chosen. Then several test runs have to be tried before a suitable load increment is found.

FCM analysis can normally be carried out by means of a general FEM program together with calculations by hand, provided that negative stiffness matrix can be solved in the program. But some special program can be more efficient when a lot of FCM calculations are to be done. In all the analyses of the report a small program developed for FCM analyses has been used.

In FCM analysis only a number of nodes, which are located along propagation path and related to determination of load and displacement, are required to be considered. Therefore, it is efficient to use a substructure element by condensing away the other nodes. The stiffness matrix can be greatly reduced.

The program used in calculations consists of mainly two parts: formulation of substructure element and FCM calculation. The first part can perform meshing, formulation of system stiffness matrix, static condensation. The second part includes solving system equations, determining load path and evaluating stresses etc., updating stiffness matrix and input.

3.4 Choice of element type

In LEFM calculations special element types, for instance singular element or distorted 8-node isoparametric element, and very fine element meshes have to be utilized in order to produce stress singularity.

In the FCM model a more realistic fracture process zone in front of the crack tip has replaced the stress singularity. Consequently it greatly reduces difficulties in FEM calculations. It is possible to use ordinary elements and relative coarse meshes to perform fracture analyses.

During the past studies mainly linear finite elements have been used. They are simple and have only corner nodes. But they are too stiff in bending and too sensitive to elongation or distortion of element form. Thus a fine mesh has to be chosen in order to obtain a satisfactory result. Then large stiffness matrix may exceed storage limit.

Higher order elements, for instance quadratic element usually yield much better results and coarse mesh can be used. But when higher order elements are used in FCM analysis problems of incompatibility can appear. As shown in Fig 3.1 incompatibility along interelement boundaries located on the crack propagation path can arise, when a node is splitted into two nodes and a spring is inserted.

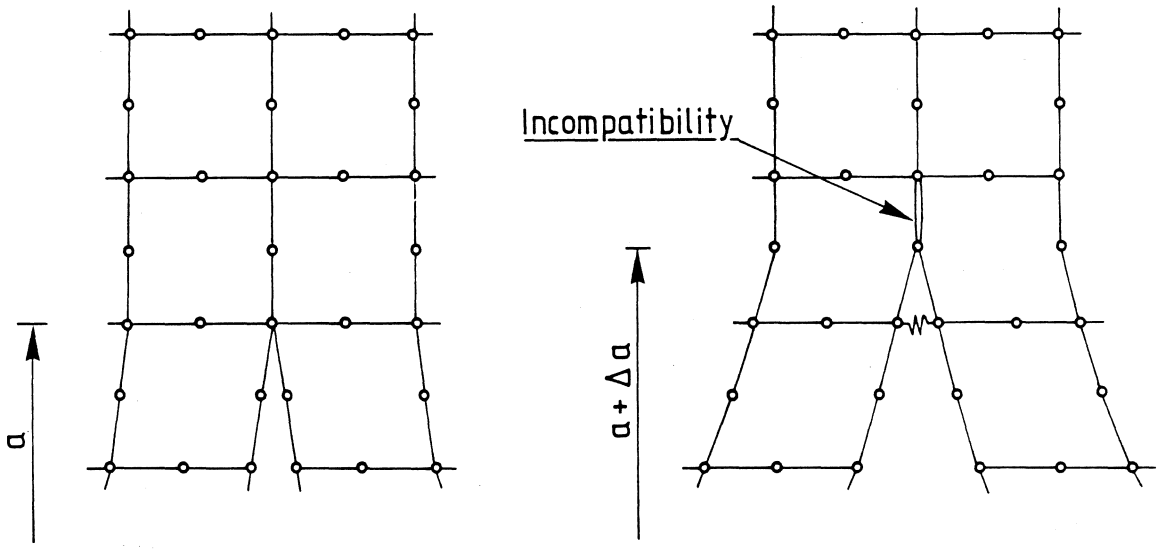

Fig 3.1 Possible incompatibility

The opening of fictitious crack for concrete materials is relatively small, at least at the first stage. In addition to it, very small load increments are chosen in FCM analysis when intensive cracking takes place. Thus, the incompatibility may be so small that influence can be negligible. On the other hand, in FEM analysis interelement incompatibility can be allowed to a certain degree. In bending problems incompatible elements can even yield better result than compatible ones. Thus one may argue that higher order elements are possible to give proper results in FCM analysis.

A numerical test has been performed to check if a higher order element can yield a reasonable result. A FCM analysis of a three-point bending test is made by means of linear elements and 8-node isoparametric ones respectively. The meshes are chosen as in Fig 3.2 a and b correspondingly. Mesh a in Fig 3.2 has been used by Petersson (37) and other reseachers and is expected to yield reliable results.

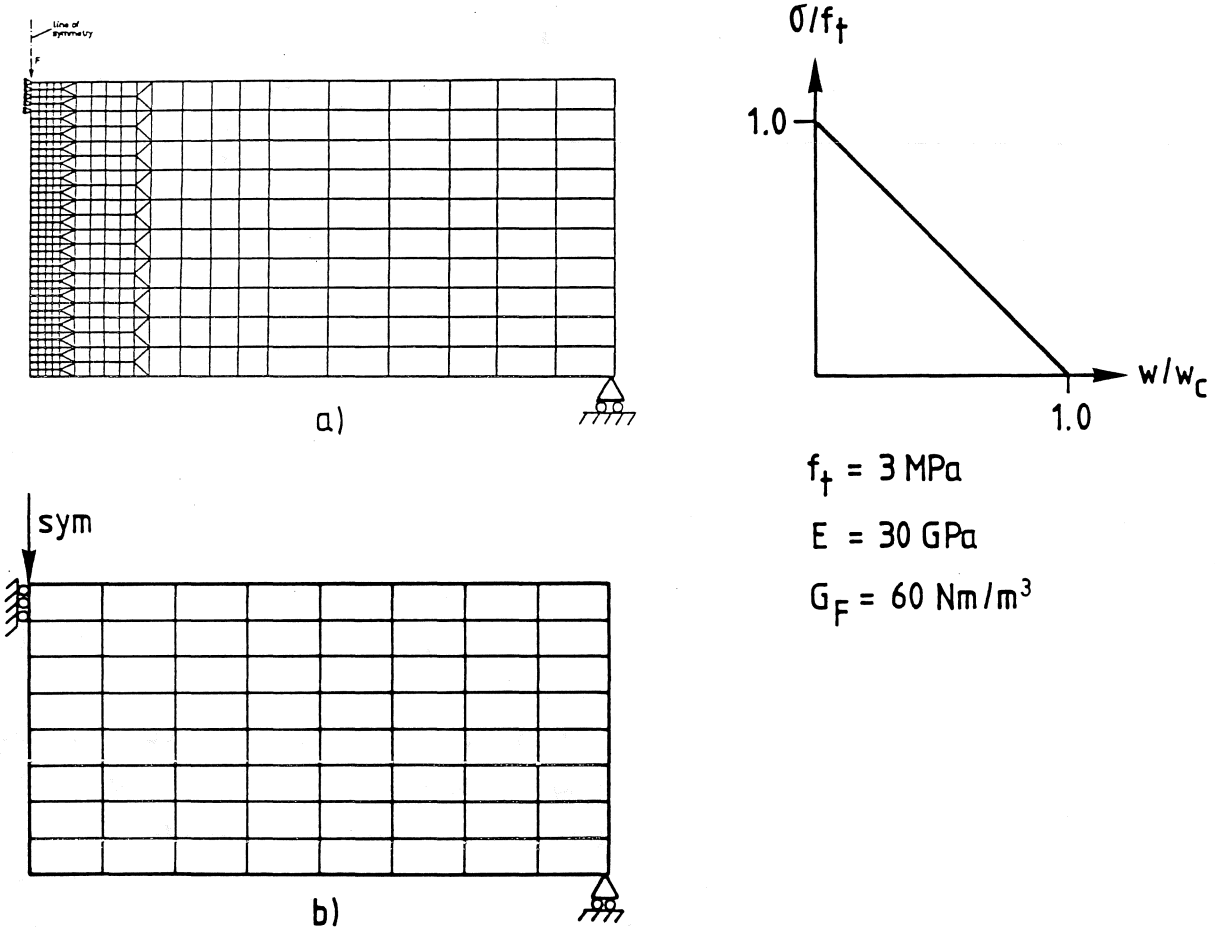

Fig 3.2 Meshes and material properties

Fig 3.3 shows the numerical result. It seems that 8-node isoparametric elements yield a proper result although a coarse mesh has been chosen.

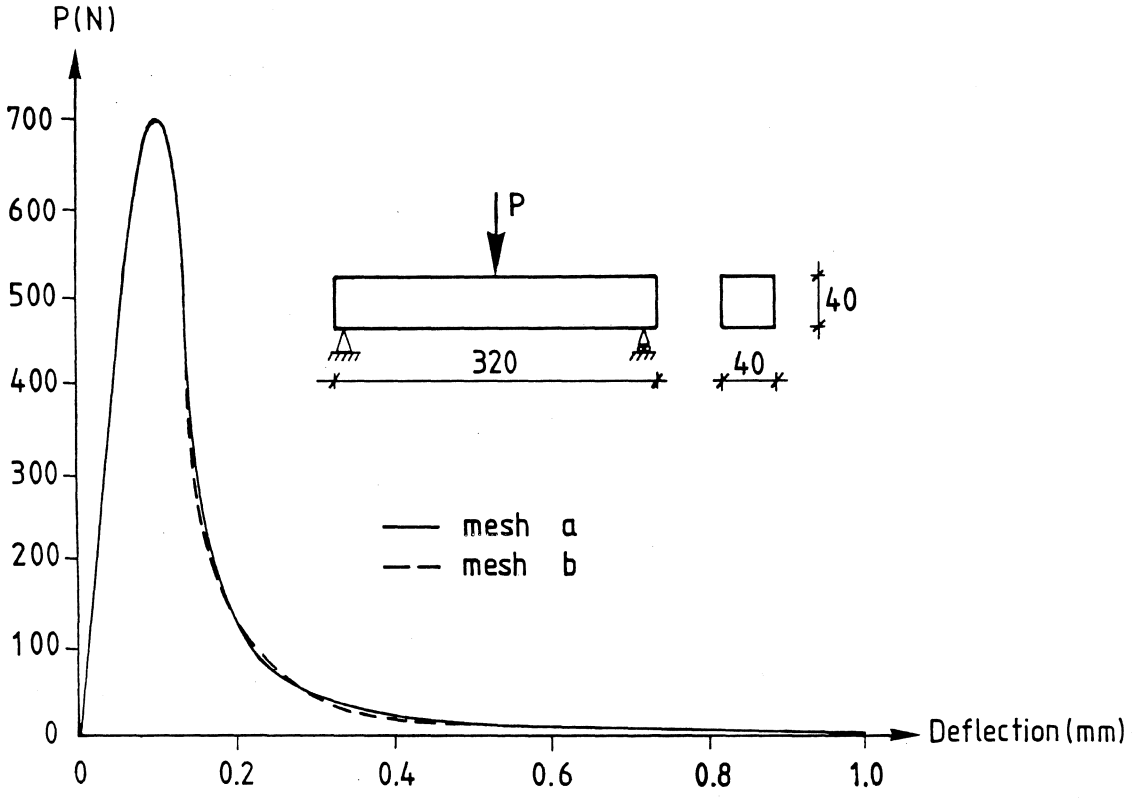

Fig 3.3 Simulating load-deflection curves with quadratic and linear elements

4 STABILITY AND VALIDITY OF DIRECT TENSION TESTS

4.1 Introduction

For non-yielding materials such as concrete, tensile fracture plays an important role in failure of concrete structures. In order to accurately predict the overall response of concrete structures, it is necessary to include the post-peak behaviour, as indicated by intensive fracture studies in recent decades.

Tensile property serves as material input for some modern fracture models, for instance the FCM model which has been applied to analyse fracture behaviour of plain and reinforced concrete structures. Not only the tensile strength f_t and fracture energy G_F, but the shape of the tensile curve can also influence structural response (7,30).

The best way to determine the tensile property may be the direct tension test. As modern closed-loop testing machines have become accessible, it is no longer difficult to carry out a complete tension test for a stress-softening material. But unfortunately a stable and reliable tensile curve in a tension test is often very difficult to obtain. Highly unsymmetric deformations in damage zones and steep stress-drops, so-called bump effect, in stress-deformation diagrams have been observed in tension tests.

In this chapter stability and validity analyses of direct tension tests are presented. The influence of eccentricity and rotation in damage zone on tensile property is investigated. The role of rotation stiffness of testing set-ups on a stable and reliable tension test is illustrated.

4.2 Stability analysis

The stress-deformation diagram obtained from a direct tension test can be regarded as material behaviour only if the stresses and deformations throughout the damage zone are uniformly distributed and the deformations keep stable increase in the whole test. In other words, only a stable translation is allowed to take place and any rotation must be prohibited inside the damage zone.

Ideally those conditions may be completely fulfilled by means of an infinite stiff testing machine provided that a very short specimen is used. In practice a testing machine has a finite tension stiffness K_t and rotation stiffness K_r (Fig 4.1.a). Thus, two types of instabilities may occur.

The first type of instability is related to realization of a stable increase in deformations inside the damage zone. A uniform distribution of stresses and deformations is assumed in this case. In a stable test no sudden jump should take place in the stress-deformation diagram. Too low K_t or too slender specimen gives rise to an unstable test. Such a type of instability can be avoided by use of a modern closed-loop testing machine if a proper deformation control variable has been chosen.

The second type denotes the rotational instability. Rotation in the damage zone can give rise to a non-uniform stress distribution and may cause unloading or compression inside the damage zone. Consequently the measured tension strength may be much lower than the real one and the stress-deformation curve may be highly distorted.

This type of instability is not well-known. In many cases bumps in stress-deformation diagrams due to rotation instability are not

very pronounced. Thus, some distorted, but still smooth stress-deformation curves, may be misintepreted as material behaviour.

Rotation of crack surfaces is almost unavoidable in direct tension tests. Possible small load eccentricity, unsymmetry of specimens and imperfection of materials can cause highly unsymmetric deformations in the damage zone. In order to obtain a reliable and stable σ-w curve, the rotation stiffness K_r of testing set-ups must be high enough to counter-act possible rotation. Of course no too slender specimen should be chosen.

But what conditions should be fulfilled for a stable test concerning possible rotation in damage zone? The following stability analysis tends to formulate a stability criterion. A theoretical analysis of the stability problem can be carried out concerning load eccentricity. All cross-sections are assumed to remain plane and a damage zone has been formed over the whole cross-section between the notches. Inside the damage zone the σ-w curve is supposed to be valid and outside, linear elastic behaviour is assumed (Fig 4.1).

Suppose that a load P located at Point B with an eccentricity e from the neutral point A and the rotation stiffness of the set-up is K_r. M_s denotes the stabilizing moment from K_r. The load P shall equal to the average stress σ in the damage zone multiplied by the area as

$$P = \sigma b_c d_c \qquad (1)$$

where b_c, d_c are the thickness and width in the zone.

Let δw represent the deformation difference between the left and right side in the damage zone (Fig 4.1.c). If a linear stress

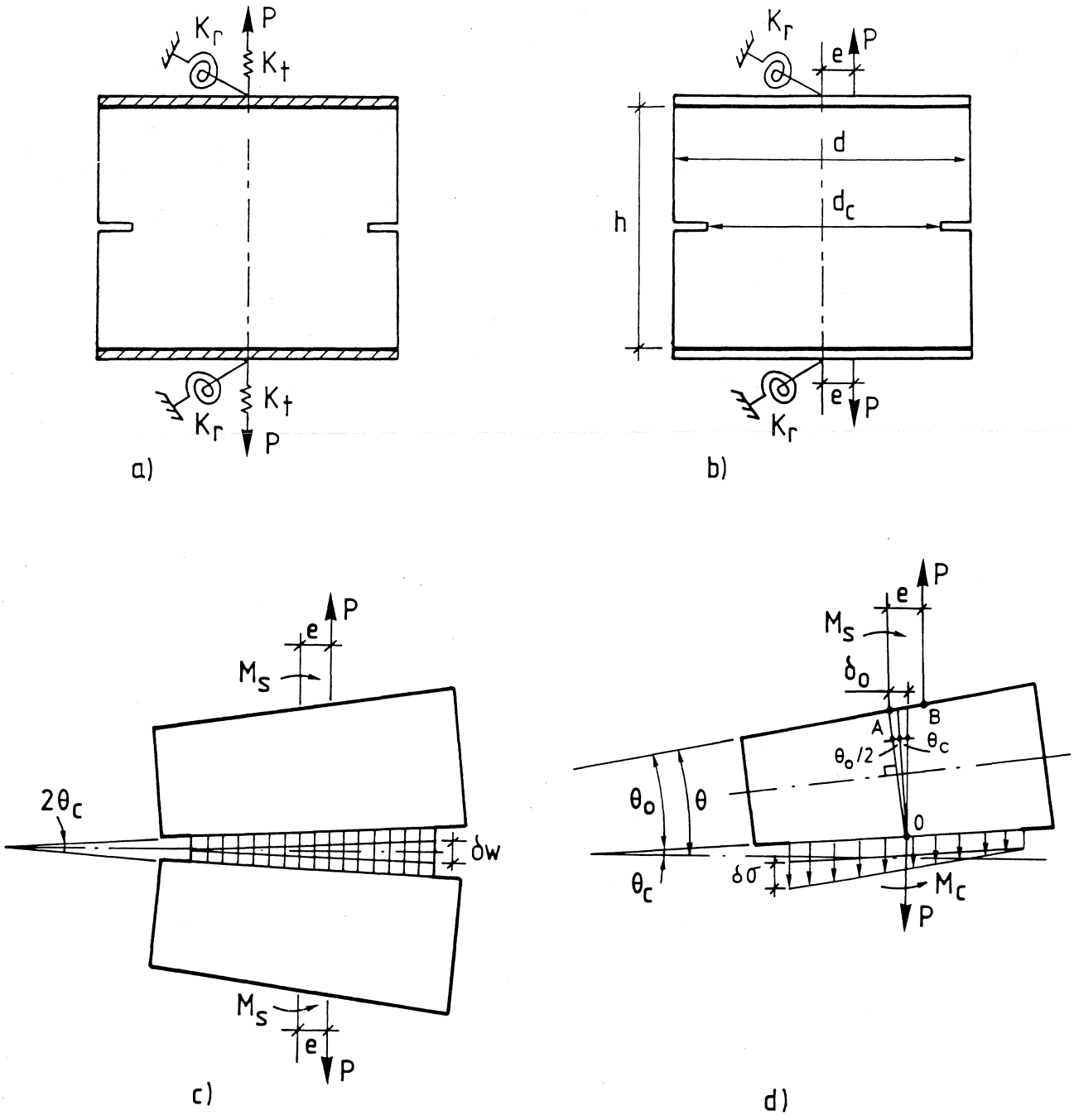

Fig 4.1 Notations for stability analysis

distribution can be approximately assumed, the corresponding stress difference $\delta\sigma$ (Fig 4.1.d) can be given by

$$\delta\sigma = (-d\sigma/dw)\,\delta w \tag{2}$$

where $(d\sigma/dw)$ is the slope in the σ-w curve and is negative.

The moment M_c in the damage zone (Fig 4.1.d) can be calculated from

$$M_c = \delta\sigma b_c d_c^{\,2}/12 \tag{3}$$

Substituting eqs. (2) into (3), yields the relation

$$\delta w = \frac{12M_c(-dw/d\sigma)}{b_c d_c^{\,2}} \tag{4}$$

Then the rotation angle θ_c of the crack surface can be given by

$$\theta_c = \frac{\delta w}{2d_c} = \frac{6M_c(-dw/d\sigma)}{b_c d_c^{\,3}} \tag{5}$$

The rotation angle θ_0 of the upper end with respect to the crack surface due to bending is

$$\theta_0 = \frac{(Pe-M_s-M_c)3h}{Ebd^3} \tag{6}$$

where b, d and h are the thickness, width of unnotched cross-section and length of the specimen respectively.

The horizontal distance δ_0 between the two points A and O is

$$\delta_0 = (\theta_c+\theta_0/2)h/2 = \frac{3M_c(-dw/d\sigma)h}{b_c d_c^3} + \frac{3(Pe-M_s-M_c)h^2}{4Ebd^3} \qquad (7)$$

The equlibrium of moments about point O gives

$$(Pe-P\delta_0)-M_s+M_c=Pe-M_s+M_c-\sigma b_c d_c \delta_0=0 \qquad (8)$$

Substituting eqs. (7) into (8), we obtain

$$(Pe-M_s)\left[\frac{2}{hb_c d_c \sigma} - \frac{3h}{2Ebd^3}\right] + M_c\left[\frac{2}{hb_c d_c \sigma} + \frac{6}{b_c d_c^3}\frac{dw}{d\sigma} + \frac{3h}{2Ebd^3}\right]=0 \qquad (9)$$

The rotation angle θ of the upper end with respect to initial state shall equal to $\theta_c + \theta_0$. The boundary condition gives

$$\theta = M_s/K_r = \theta_c + \theta_0 \qquad (10)$$

Substituting eqs. (5), (6) and (1) into (10), we obtain

$$(Pe-M_s)\left[\frac{1}{K_r} + \frac{3h}{Ebd^3}\right] - M_c\left[\frac{6}{b_c d_c 3}\frac{dw}{d\sigma} + \frac{3h}{Ebd^3}\right] = \frac{\sigma b_c d_c e}{K_r} \qquad (11)$$

Solving the eqs. (9) and (11), $(Pe-M_s)$ can be given as

$$(Pe-M_s)= -\frac{2}{\det}\frac{e}{K_r h}\left[1 + \frac{3h}{d_c}\frac{\sigma}{d_c}\frac{dw}{d\sigma} + \frac{3\sigma}{4E}\frac{h^2 b_c d_c}{bd^3}\right] \qquad (12)$$

where det is the determinant of the coefficient matrix and is given by

$$\det = -\frac{2}{hb_cd_c\sigma}\frac{1}{K_r}\left[1+\frac{3h}{d_c}\frac{\sigma}{d_c}\frac{dw}{d\sigma}+\frac{3\sigma}{4E}\frac{h^2b_cd_c}{bd^3}\right]-\frac{2}{hb_cd_c\sigma}\frac{6h}{Ebd^3}$$
$$-\frac{2}{hb_cd_c\sigma}\frac{6}{b_cd_c^3}\frac{dw}{d\sigma}\left[1+\frac{3\sigma}{4E}\frac{h^2b_cd_c}{bd^3}\right] \quad (13)$$

In tension tests the sizes h,b,d,b_c,d_c have the same order of about 0.05 m. For concrete materials $\sigma \approx 3$MPa, $E \approx 30$GPa, $dw/d\sigma \approx -20\mu$m/MPa, then $\sigma/E \approx 10^{-4}$, $(\sigma/d_c)(dw/d\sigma) \approx -10^{-3}$. Therefore, the eqs. (12) and (13) can be reasonably simplified as

$$(Pe-M_s) = -2e/(\det*K_rh) \quad (14)$$

and

$$\det = -\frac{2}{hb_cd_c\sigma}\left[\frac{1}{K_r}+\frac{6h}{Ebd^3}+\frac{6}{b_cd_c^3}\frac{dw}{d\sigma}\right] \quad (15)$$

In order to obtain a real and stable direct tension test, a rotation should be able to be prevented. That is to say, the stabilizing moment should be at least greater than the moment due to eccentricity. The stability criterion may be given as

$$M_s \geq Pe \quad (16)$$

That is

$$(Pe - M_s) = -2e/(\det*K_rh) \leq 0 \quad (17)$$

If the above inequality shall be fulfilled, then

$$\det > 0 \quad (18)$$

Inserting (15) into (18), we obtain a formula for the stability criterion:

$$\frac{1}{\frac{1}{K_r} + \frac{6h}{Ebd^3}} > -\frac{b_c d_c^3}{6}\frac{d\sigma}{dw} \tag{19}$$

The rotation stiffness K_r should satisfy the following relation for $(-dw/d\sigma)_{min}$:

$$\frac{1}{K_r} < -\frac{6h}{Ebd^3} + \frac{6}{b_c d_c^3}\left(-\frac{dw}{d\sigma}\right)_{min} \tag{20}$$

If the right side is less than 0, apparently it is impossible to fulfill the inequality above since $K_r > 0$. Thus, the size of specimen should be properly chosen so that the following condition

$$\frac{hb_c d_c^3}{bd^3} < E\left(-\frac{dw}{d\sigma}\right)_{min} \tag{21}$$

can be satisfied if a stable test is possible to be performed. Otherwise, no reliable test could be carried out no matter how high the rotation stiffness would be imposed.

4.3 Evaluation of tension tests

4.3.1 Notch Sensitivity

Small errors may arise due to introduction of initial notches if a double notched specimen is used in a tension test. Such an effect is investigated by changing notch depth. The geometry and size of specimen as well as material properties are illustrated in Fig 4.2.

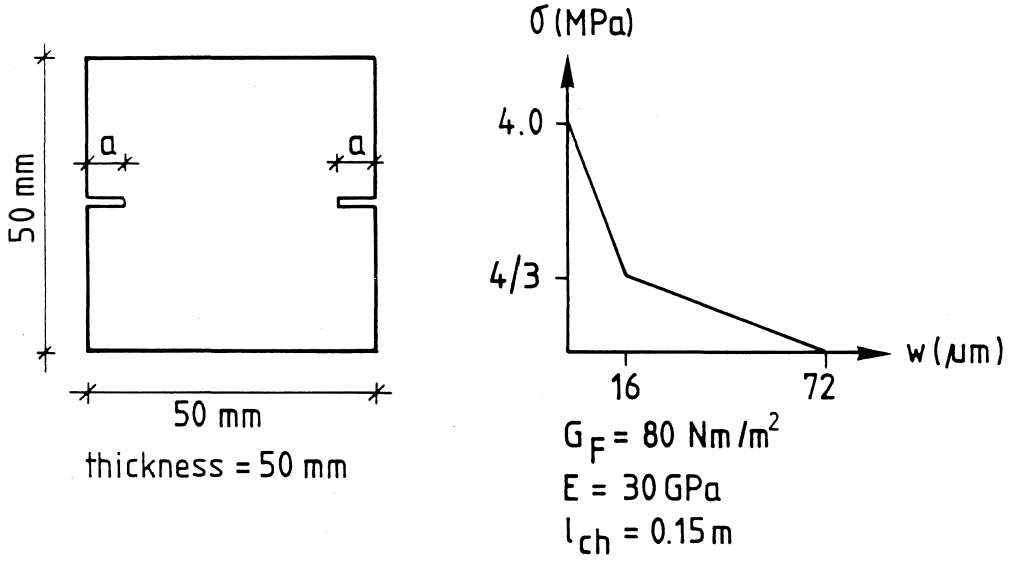

Fig 4.2 Geometry and size of specimen and σ-w curves used in the notch sensitivity analysis

Numerical results indicate that notches have very small influence on the stress-deformation curve. Only a little disturbance just before the peak-point can be observed (Fig 4.3). In tension tests of rock material by Labuz et al.(29), the experimental results seem to confirm this observation (Fig 4.4).

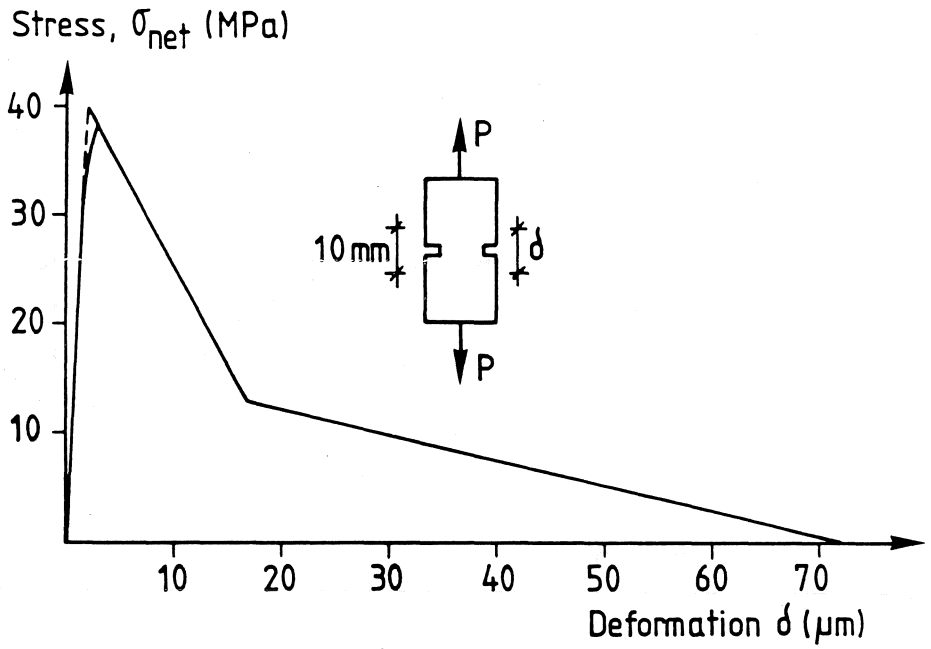

Fig 4.3 Simulating σ-w curve of a tension test.
Notch depth a=5mm

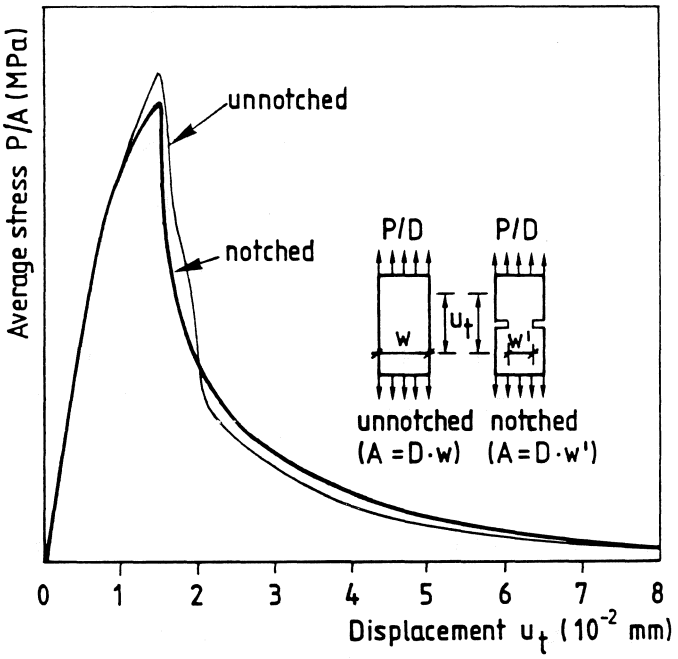

Fig 4.4 Experimental curves of notched and unnotched specimens after Labuz et al.

Inside the damage zone the stress-distribution is uneven in the pre-peak stage. But it tends to be more even as stresses increase. Just past the peak-point a uniform stress-distribution can be obtained (Fig 4.5).

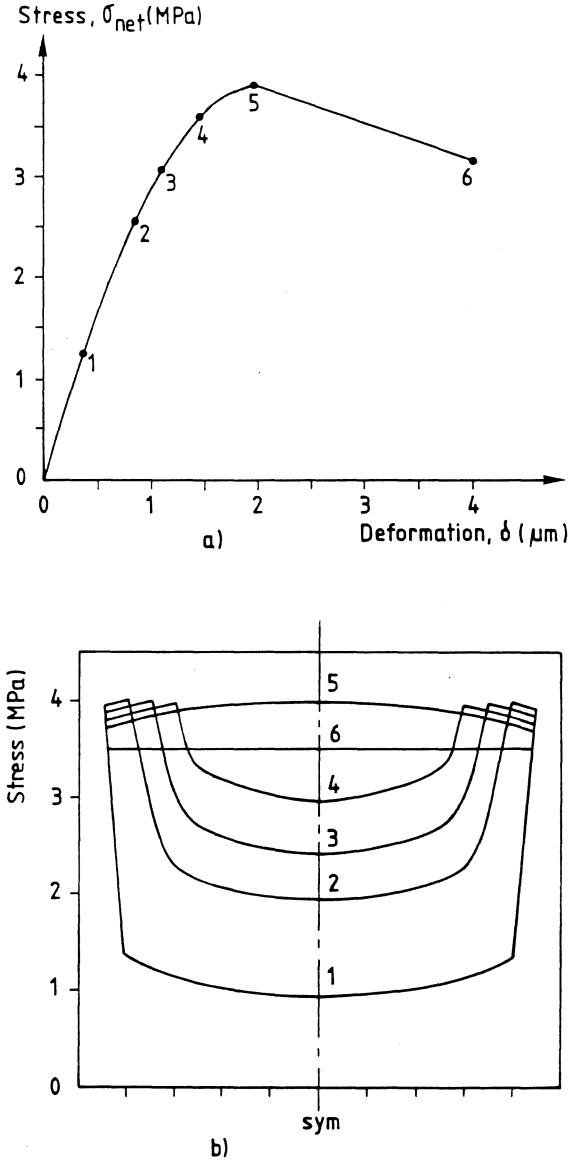

Fig 4.5 (a) Enlarged part of the stress-deformation curve in Fig 4.3
(b) Stress-distribution over the damage zone

The notch sensitivity of tensile strength is depicted in Fig 4.6. When the notch depth changes from 0 to about 25% of specimen width, the strength decrease reaches a maximum. But if there is a further increase of the notch depth, the strength decrease tends to diminish.

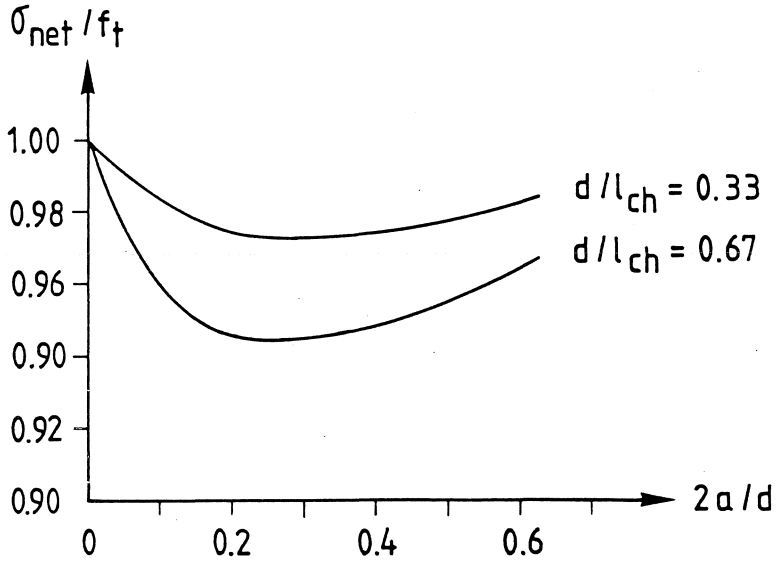

Fig 4.6 Notch Sensitivity

It can be expected that tensile strength becomes more sensitive to notches if the material is more brittle for the same specimen. But even if the characteristic length l_{ch} of the material is halved, the maximum strength decrease is only about 6%. For concrete materials l_{ch} may change from 0.1 m to 0.4 m, therefore it seems to be reasonable to conclude that the use of notched specimens does not cause great error provided the size of specimens in tests is not too large.

4.3.2 Eccentricity and Rotation

In tension tests performed by Hordijk et al., steep stress-drops or so-called bumps have been observed in the stress-deformation diagrams, although the load and displacements could be controlled properly. The deformation distribution over the cross-section between notches keeps uniform until the peak-point, and becomes highly rotated when the bump occurs, hereafter the distribution tends to become more even. Both in-plane and out-of-plane rotations have been observed. A remarkable example is shown in Fig 4.7.

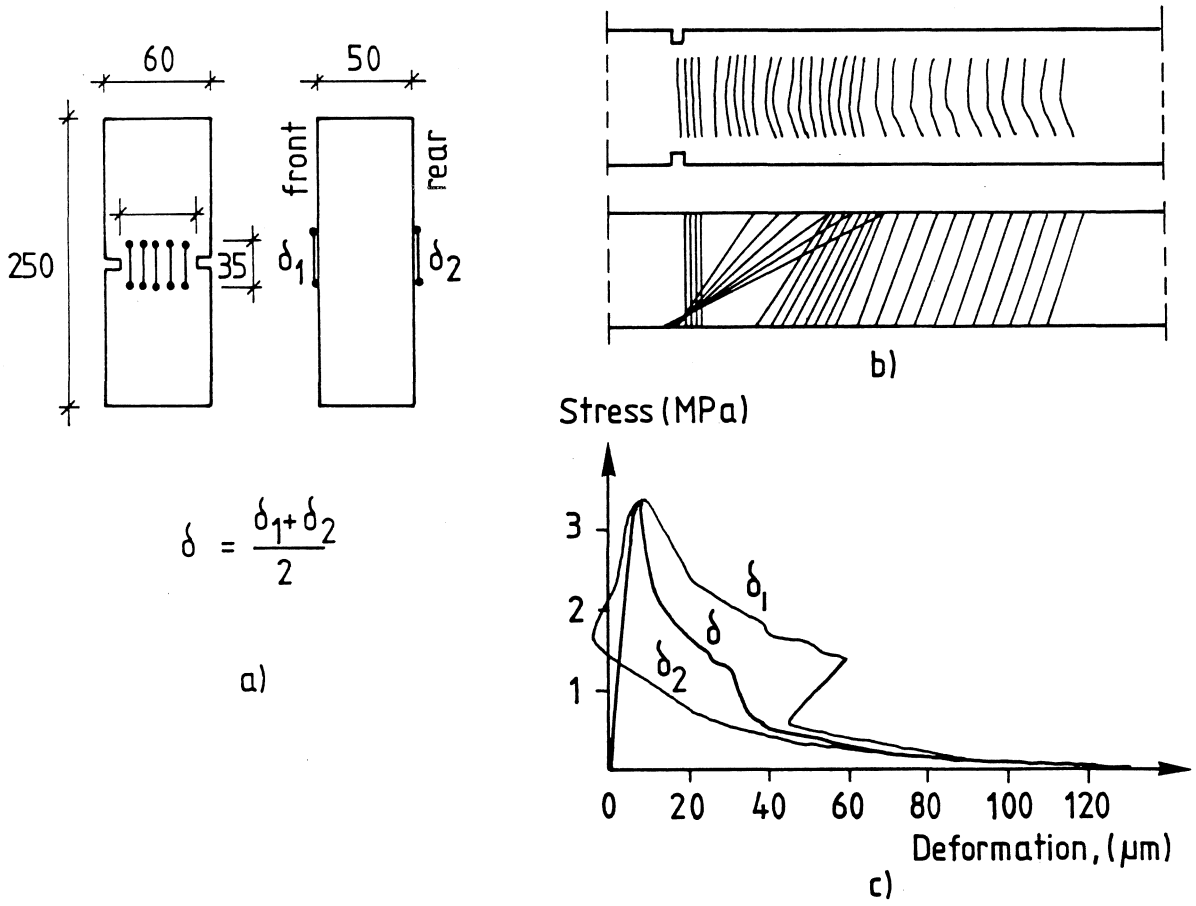

Fig 4.7 A tension test after Hordijk et al.

In tests by Van Mier et al., both double and single notched specimens were used to investigate possible structural behaviour due to unsymmetric notches (Fig 4.8). A more notable bump effect has been observed. The deformations on one side increase more quickly than the ones on the opposite side and even compressive strains arise. It seems to suggest that the crack surfaces rotate towards each other.

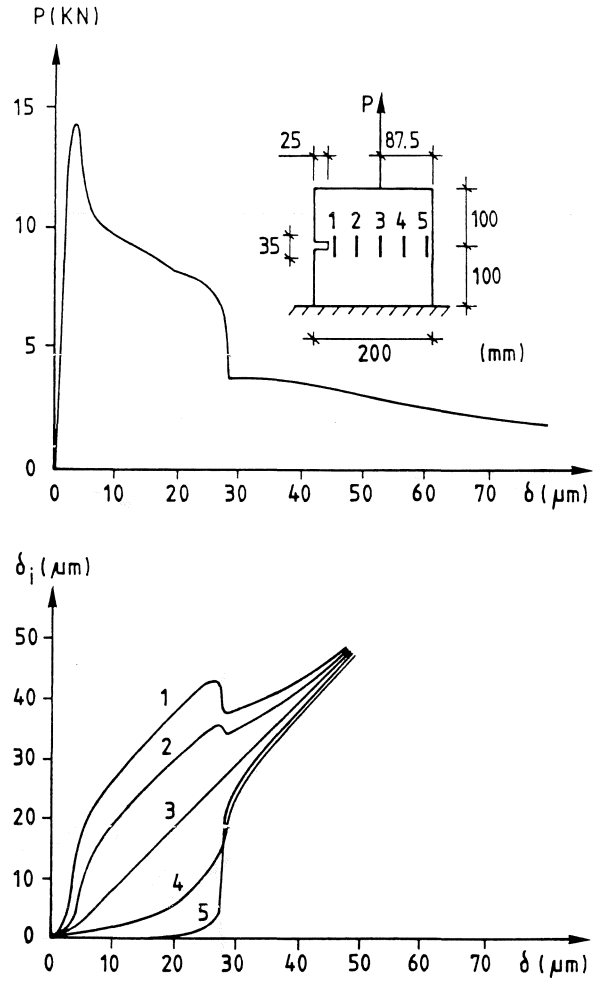

Fig 4.8 A tension test with an unsymmetric notched prism after Van Mier et al. δ is derived from LVDT measurement along the load line (in 65 mm length)

It seems that the bump effect may be highly related to the rotation in the damage zone. In tests rotation may be caused by a small load eccentricity, unsymmetry of specimens, material imperfection an so on. It seems to be of great interest to analyse the effect of rotation in the damage zone on a direct tension test, and the role of boundary condition in a reliable test. The analyses focus mainly on rotation caused by an initial load eccentricity. An attempt is to analyse the effect of rotation on the σ-w curve and possibility of eliminating the effect by imposing certain boundary conditions to prevent the rotation, as well as to qualitatively illustrate the bump effect in tests.

The specimen geometry and size are shown in Fig 4.9. Three forms of σ-w curves, one linear and two bilinear ones, are chosen. The eccentricity e changes from 1 mm to 2.5 mm.

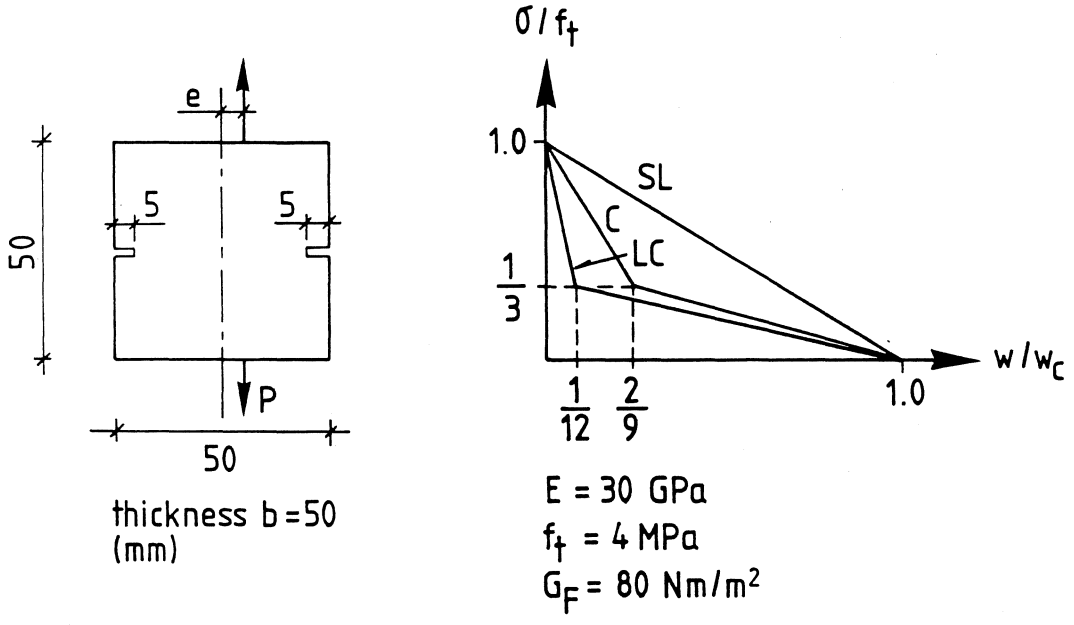

Fig 4.9 Load configuration, specimen size and σ-w curves used in analysis. SL: straight line; C: concrete; LC: light-weight concrete

(1) Free Rotation

The rotation stiffness of the testing set-up is assumed to be zero. The material curve C is used.

Fig 4.10 presents the influence of eccentricity on the σ-w curves. The curves deviate greatly from the real material behaviour. As the eccentricity e increases to 2.5 mm, the measured strength decreases to 75% of the real strength. The strength loss can reach more that 10% only for a load eccentricity e=1 mm!

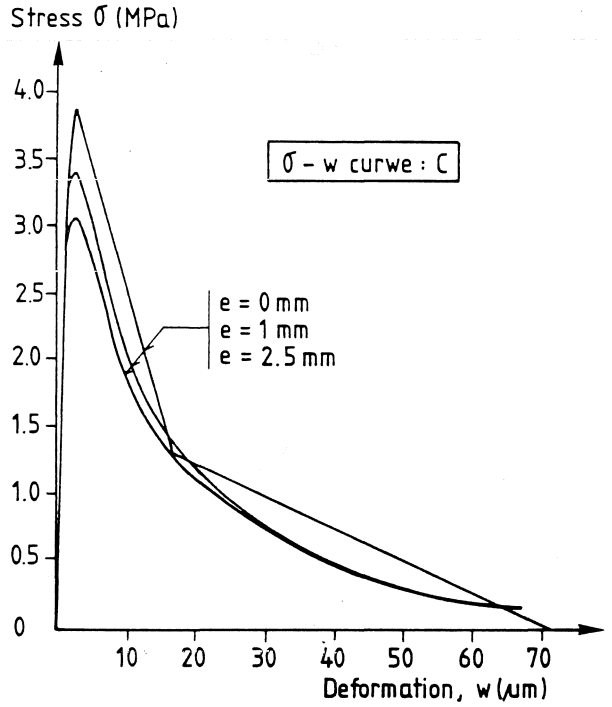

Fig 4.10 Influence of eccentricity on σ-w curves

Since linear elastic behaviour is assumed outside the damage zone, the fracture energy G_F should be equal to the external work. The external work should be the same for the same crack area. But it seems unreasonable that the area under the calculated σ-w curve

(Fig 4.10) decreases as eccentricity increases. The possible explanation is that the measured deformation is not equal to the deformation along the load line if a load eccentricity occurs. Thus, the area under the measured stress-deformation curve is not equal to the external work.

In a tension test the deformation is often measured from the average value of displacements in between the notches on both sides. But when a rotation occurs, unloading or compression can arise in the damage zone even if the average deformation keeps increasing (Fig 4.11). The stresses and deformations are highly nonuniformly distributed, the rotation in the damage zone keeps increasing (Fig 4.12). It suggests that tension-bending failure takes place instead of a real direct tension fracture. Apparently, the measured response cannot represent the real material behaviour.

No bump effect has been observed in the calculated stress-deformation curves for free rotation, although the curves have indeed distorted.

A small eccentricity is apt to take place in a direct tension test. Thus, it seems impossible to obtain a reliable material test, though a smooth curve may still be measured, if no measures have been taken to counteract the rotation in the damage zone.

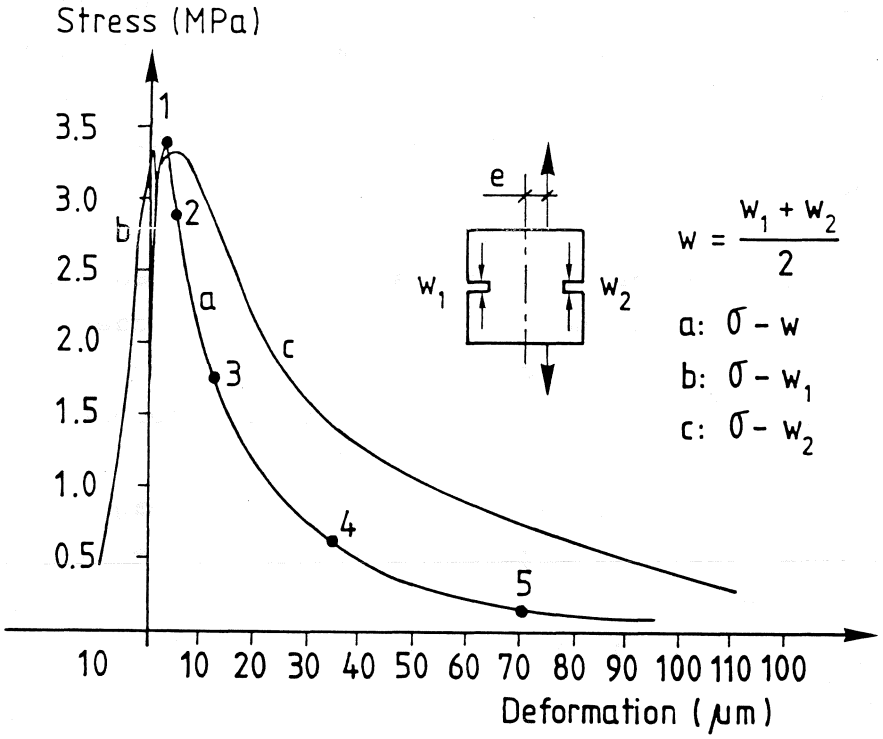

Fig 4.11 Average and local σ-w curves.
K_r=0 MNm/rad, e=1 mm.

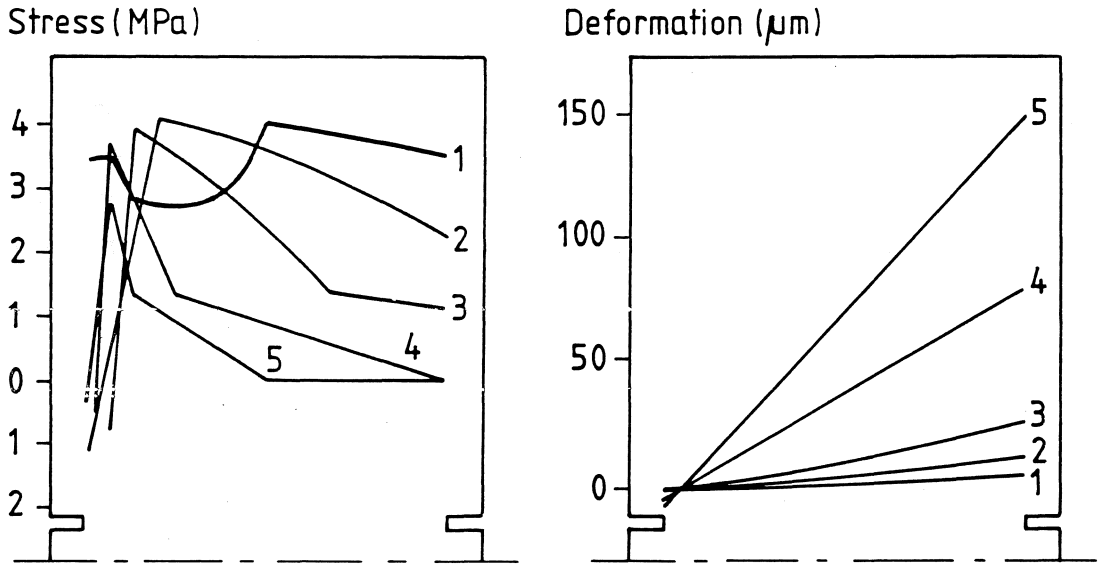

Fig 4.12 Stress and deformation distributions.
K_r=0 MNm/rad, e=1 mm.

(2) Role of rotation stiffness

A certain boundary condition must be imposed to prevent the rotation for a reliable tension test. A testing set-up for mixed mode fracture, developed mainly by Hassanzadeh, at the Division of Building Materials, Lund Institute of Technology, is to be used to demonstrate the important role of rotation stiffness in tension tests. The set-up is made of two steel beams connected by a thin steel plate and some parts for shear measurement (Fig 4.13 a).

The rotation stiffness K_r can be approximately calculated by

$$K_r = M/\theta = 3E_{st}I/L$$

where E_{st} is the modulus of steel, I is the moment of inertia of the beam and L is the length (Fig 4.13 b,c).

The set-up should not give rise to great errors provided that the beam is not too short. A test is made to investigate if the set-up can influence the translation in the damage zone. K_r is 0.2 MNm/rad and the material curve C is used. The result for no eccentricity is shown in Fig 4.14. The calculated stress-deformation replicates the input material curve. Hardly any unsymmetric stress distribution can be found before the last deformation stage. It seems that the set-up does not cause any notable error.

For material C the maximum value of $-(d\sigma/dw)$ is $1.667 \cdot 10^{11}$ Pa/m. According to the stability criterion, inequality (19) K_r should be greater than about 0.1 MNm/rad for the size of specimen in Fig 4.9. The eccentricity e is 1 mm.

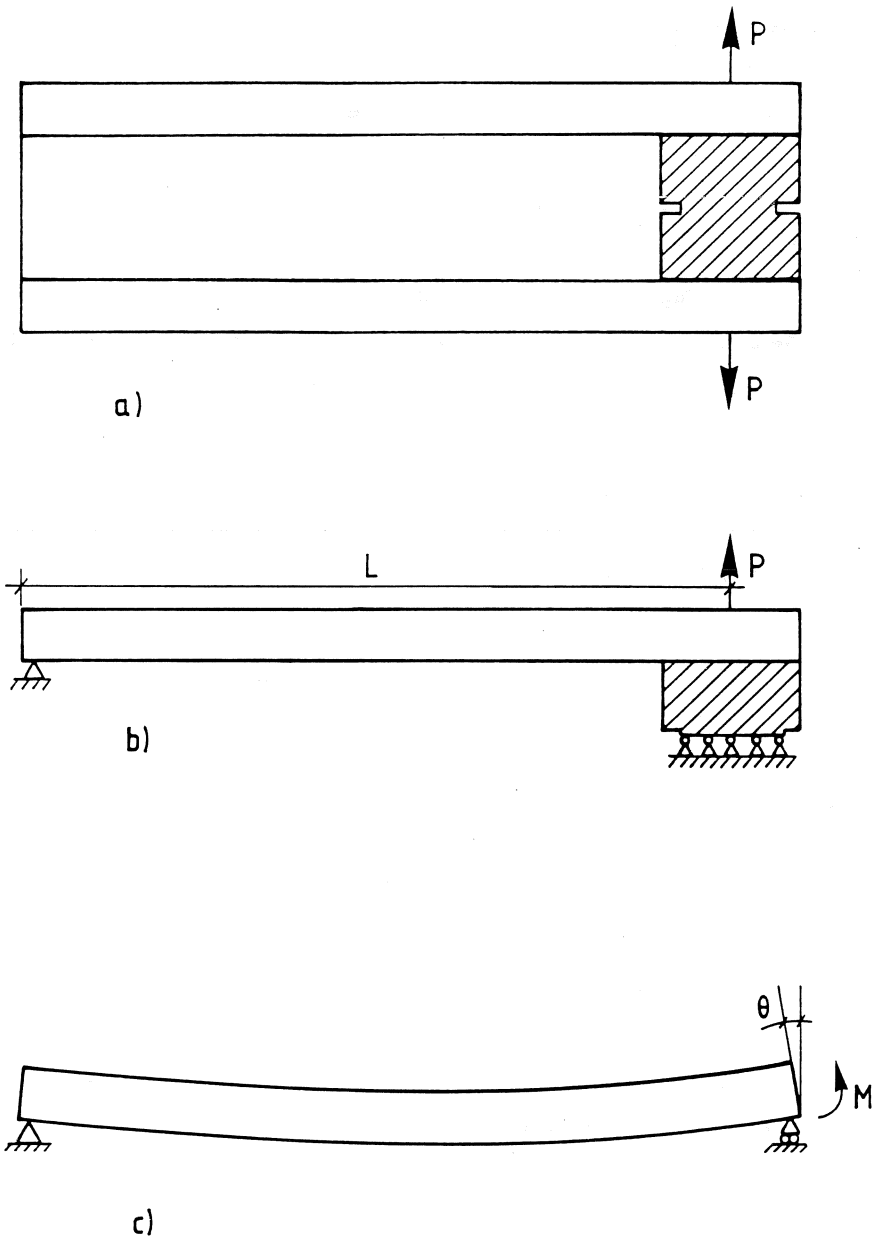

Fig 4.13 a) An arrangement for mixed mode tests by Hassanzadeh. The shear part is not shown.
b) Simplified configuration for calculations
c) Rotation stiffness of the steel beam

Two tests are calculated for K_r = 0.05 and 0.2 MNm/rad. For K_r = 0.05 MNm/rad a little lower strength and disturbance can be observed. As the rotation stiffness increases to 0.2 MNm/rad, the calculated stress-deformation curve is almost identical to the input one. The tensile strength increases from 3.7 MPa for K_r = 0.05 Mnm/rad to 3.9 MPa for K_r = 0.2 Mnm/rad. The calculated fracture energy G_F is 80 Nm/m^2 for both cases (Fig 4.15).

For K_r = 0.05 MNm/rad the stress and deformation distributions are still nonuniform just after the peak-point, but tend to become more even afterwards (Fig 4.16). But if the rotation stiffness is high enough, the rotation in the damage zone can almost be prevented. For K_r = 0.2 MNm/rad the stress and deformation distributions are uniform (Fig 4.17).

It seems that the stability criterion can give a proper prediction to rotation instability problems. If the rotation stiffness is high enough, possible influence caused by load eccentricity can be eliminated.

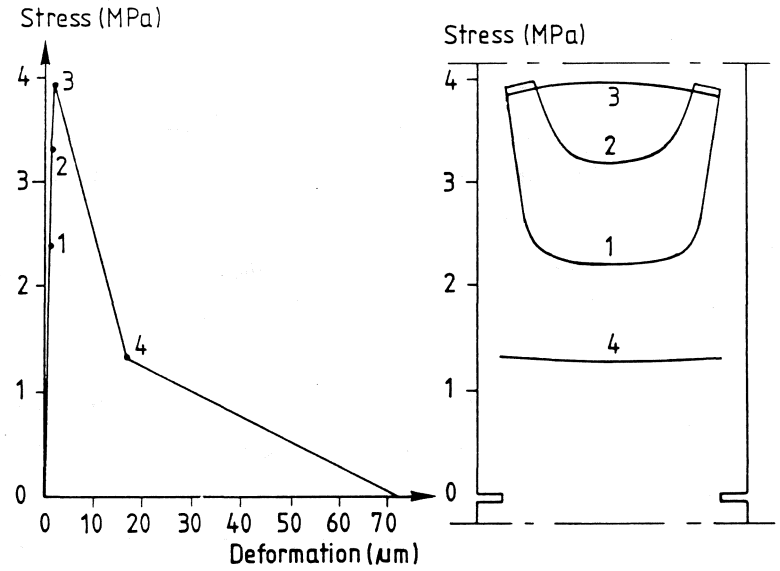

Fig 4.14 Stress-deformation curve and stress distribution for material C. K_r = 0.2 MNm/rad, e = 0 mm.

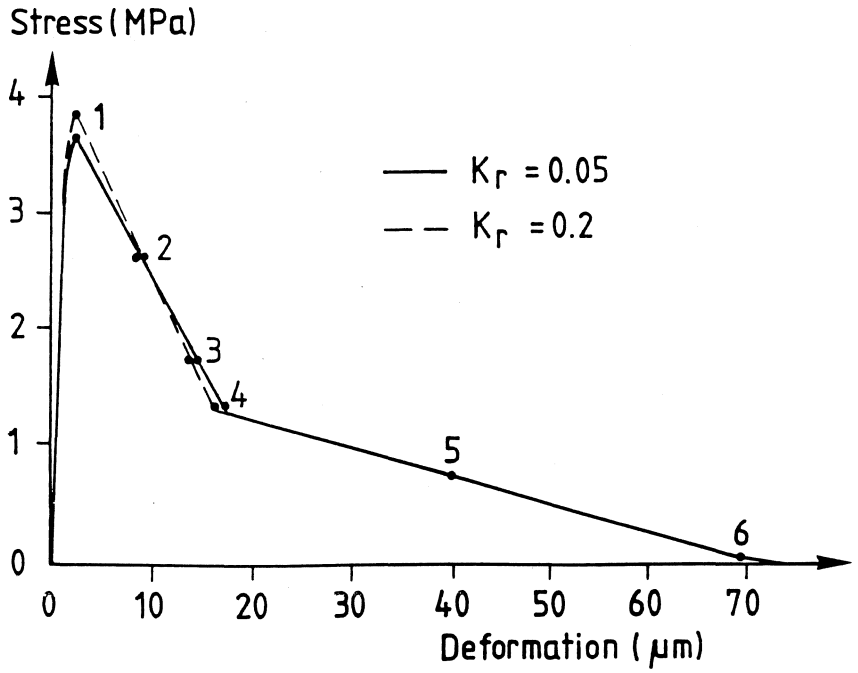

Fig 4.15 Stress-deformation curves for material curve C K_r = 0.05, 0.2 Mnm/rad, e = 1 mm.

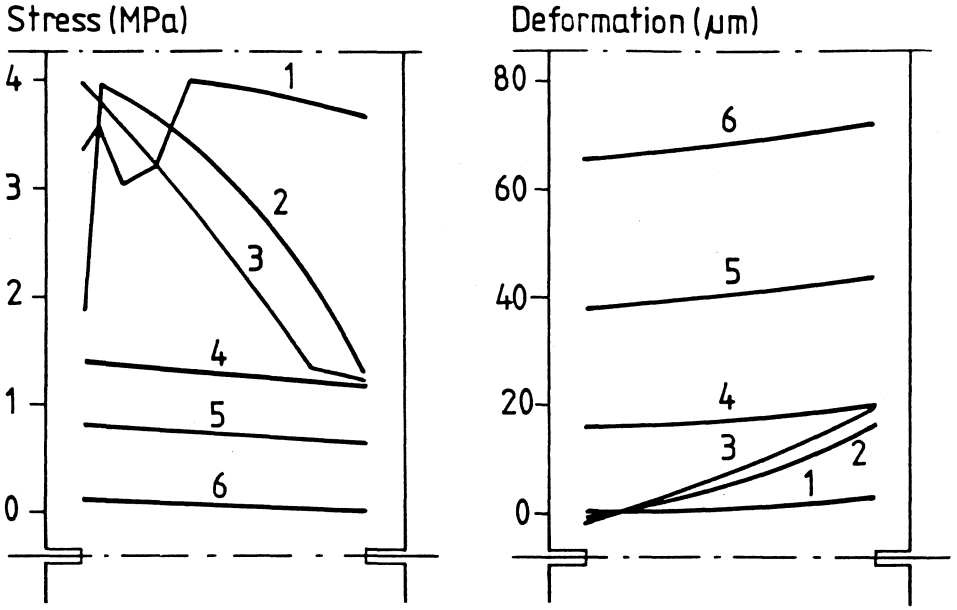

Fig 4.16 Stress and deformation distributions.
K_r = 0.05 MNm/rad, e = 1 mm.

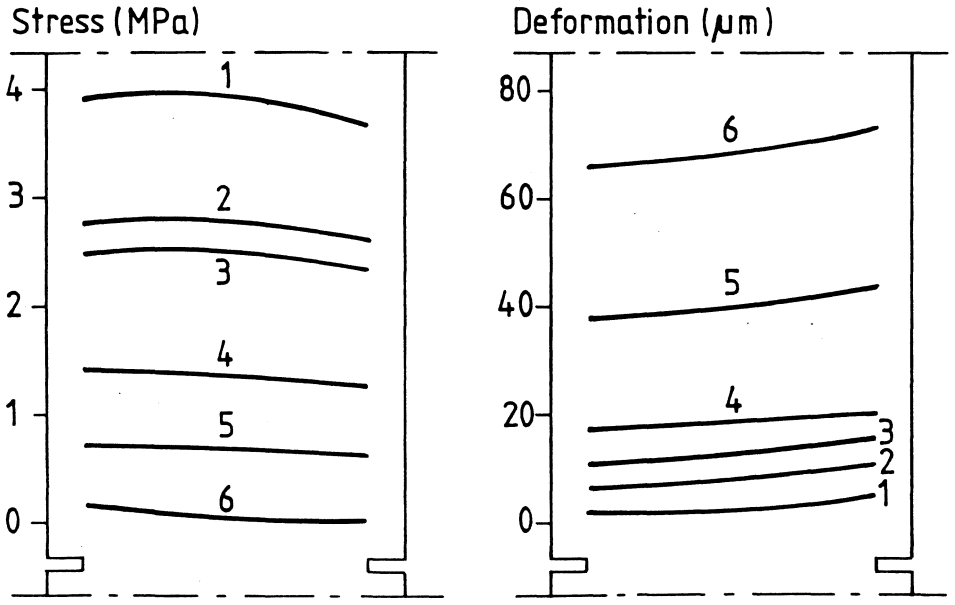

Fig 4.17 Stress and deformation distributions.
K_r = 0.2MNm/rad, e = 1 mm.

(3) Role of material property

In rotation instability, the slope $(-d\sigma/dw)_{max}$ has significant influence. Three different forms of σ-w curves for the same G_F = 80 Nm/m^2, material curves SL, C and LC (Fig 4.9) are chosen to illustrate the influence. The $(-d\sigma/dw)$ values are $1 \cdot 10^{11}$, $1.667 \cdot 10^{11}$ and $3.333 \cdot 10^{11}$ Pa/m. The eccentricity e is 1 mm and K_r is 0.05 MNm/rad.

Fig 4.18 presents the result. As the slope $(-d\sigma/dw)$ increases the tensile strength decreases and the bump effect becomes more remarkable for the same boundary condition.

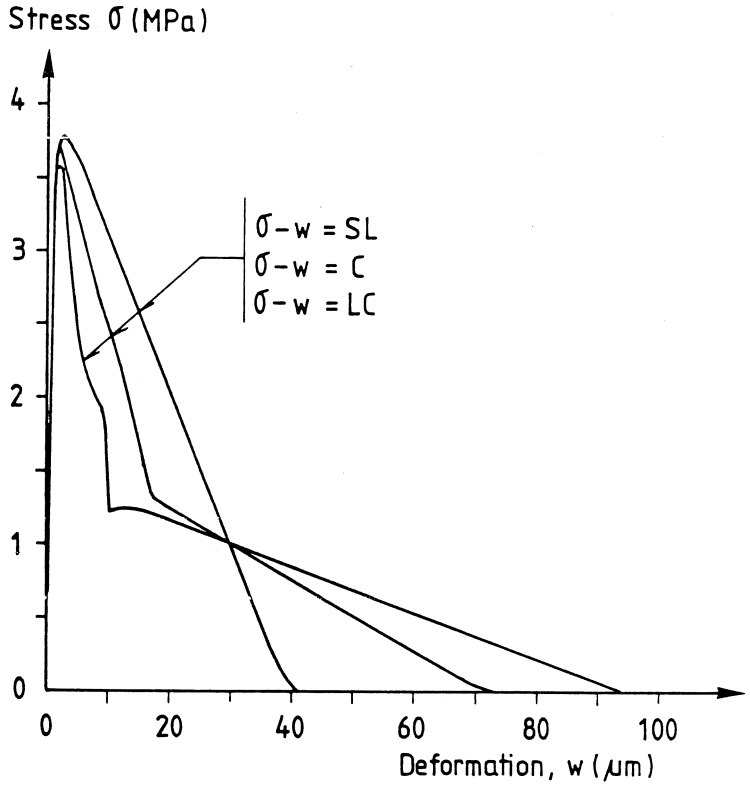

Fig 4.18 Material property and stability.
K_r = 0.05 MNm/rad

(4) Bump Effect

In numerical analyses bumps have not occurred when rotation in damage zone takes place freely. On the other hand, if the rotation is completely prevented, no bump should occur either. Therefore, it seems that bumps can probably become more remarkable for intermediate rotation stiffness. To confirm this the following analysis is performed.

For the same specimen shown in Fig 4.9, the analysis is carried out for material LC with steep slope in the σ-w curve. The rotation stiffness K_r is chosen as 0., 0.05 and 0.2 MNm/rad. The eccentricity e is 1 mm.

In Fig 4.19 for K_r = 0.2 MNm/rad the calculated stress-deformation curve is almost identical to the input curve except for a little strength loss at the peak-point. Because the rotation stiffness is

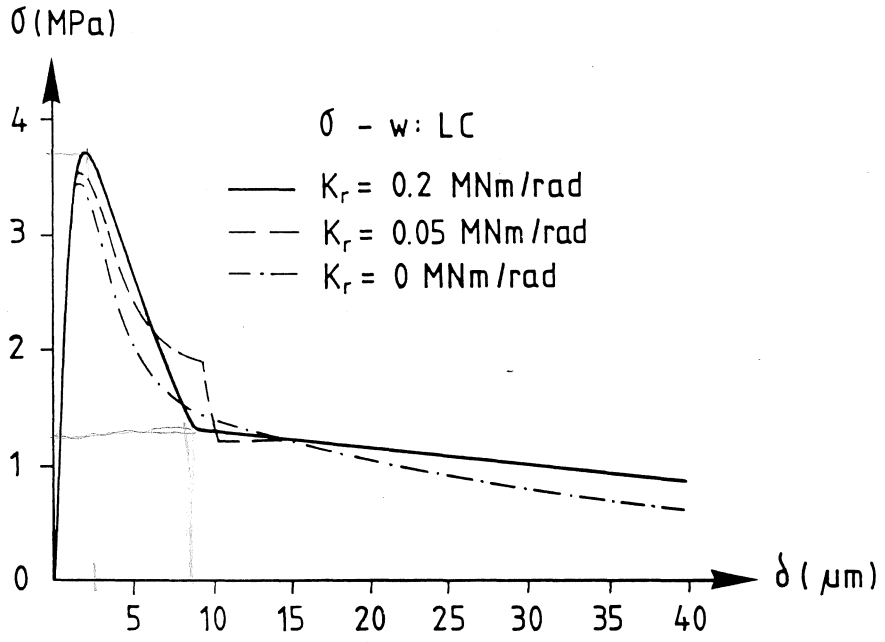

Fig 4.19 Bump effect and rotation stiffness. e = 1 mm.

still slightly lower than 0.25 MNm/rad determined according to the stability criterion, inequality (19). For free rotation K_r = 0 MNm/rad the calculated curve is smooth and no bumps occur, although the curve is distorted. But for K_r = 0.05 MNm/rad, the bump effect can be observed.

Fig 4.20 a presents the average stress-deformation curve and the stress-deformation curves on both sides. The deformation on the side near to the load line keeps increasing, and it decreases when the stress-drop occurs, whereafter it increases again. The deformation on the other side decreases after the peak-point and becomes negative, later on it increases again. Fig 4.20 a and b show that the stress-drop is strongly interrelated to a great rotation change. The result seems to agree well with the experimental observation in Fig 4.7 (Hordijk).

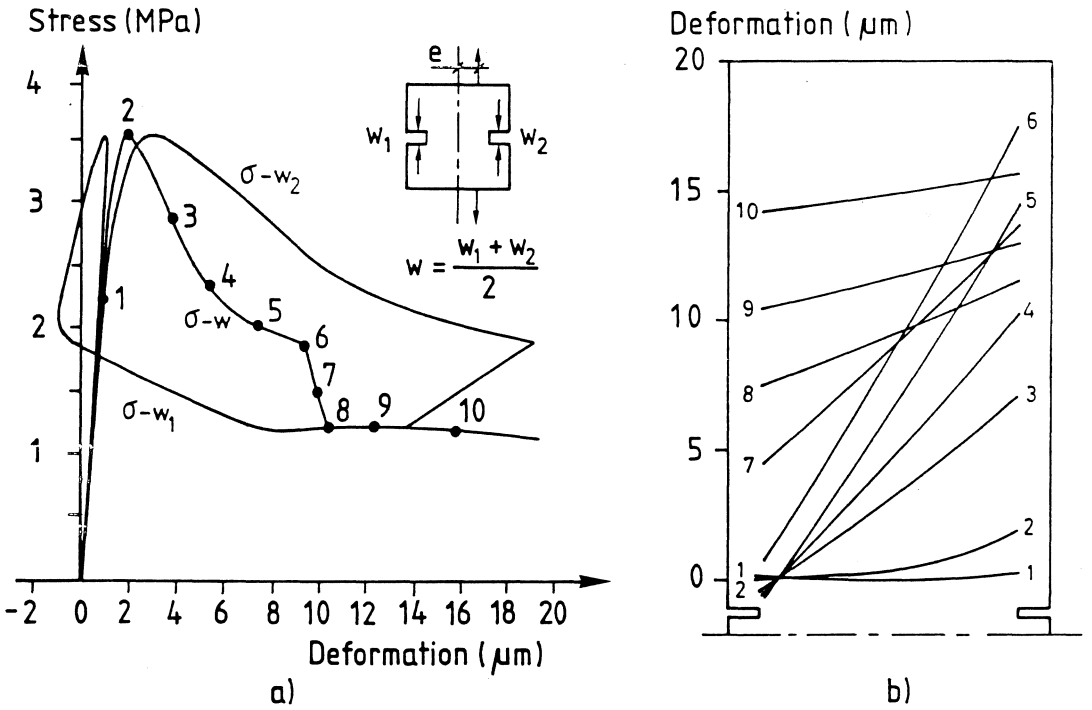

Fig 4.20 Stress-deformation curve and deformation distribution. K_r = 0.05 MNm/rad, e = 1 mm.

In Fig 4.21 the local deformations over 2.5 mm length across the damage zone plot versus the average value of deformations measured between the notches on both sides. The result shows a similar trend to the experimental result for unsymmetric notched specimen by Van Mier et al. (Fig 4.8). It may suggest that the rotation caused by unsymmetry of specimen has a similar effect to the rotation caused by load eccentricity.

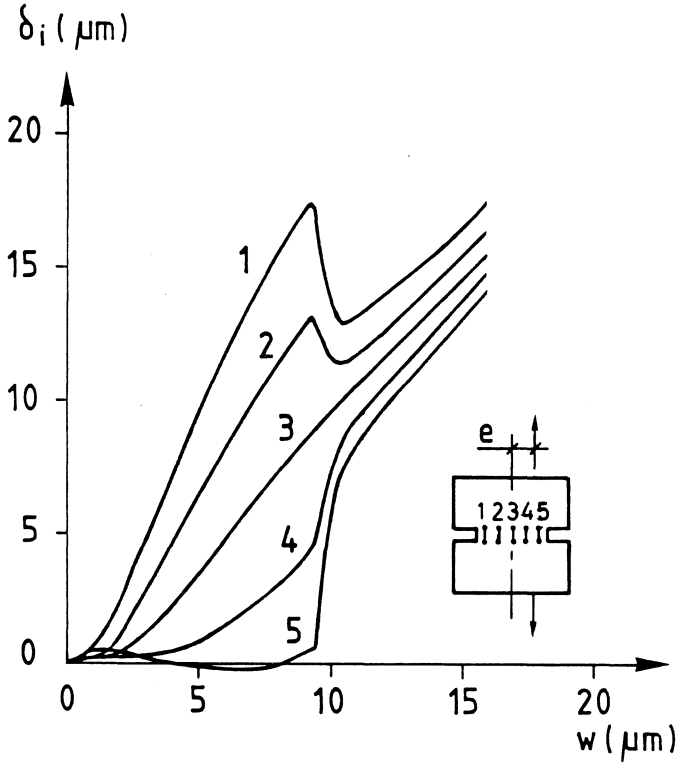

Fig 4.21 Local deformations versus average deformation.
K_r = 0.05 MNm/rad, e = 1 mm.

5 MATERIAL PARAMETERS AND STRUCTURAL BEHAVIOUR

5.1 Introduction

According to traditional strength theories based on the pre-peak stress-strain relations, structural behaviour under tensile fracture is related solely to tensile strength. But as indicated by recent fracture studies, structural behaviour should be related to a combined parameter, the so-called brittleness number d/l_{ch}.

For a given material a structure may behave from brittle to tough by changing only the charateristic dimension d of the structure with the same geometry. On the other hand the structural behaviour may be highly varied by changing the fracture energy G_F for a given structure even if the tensile strength has hardly changed.

The influence of the characteristic dimension d on load bearing capacity of a structure, referred to as size effect, has been intensively studied recently. Studies of relations between ultimate load bearing capacity and the characteristic length l_{ch} may also be of practical importance. It may serve as a tool for prediction and a guide for improvement of material behaviour.

A number of tests with various materials have been performed by use of both statically determinate and indeterminate specimen structures, and compared to the theoretical analysis by means of the FCM model. The primary objective of the tests is to theoretically and experimentally investigate the influence of material parameters on structural behaviour, and gain some insight into applicability of the Fictitious Crack Model.

5.2 Research program

5.2.1 Specimens and testing procedures

(1) Determination of material parameters

For plain concrete materials the shape of the σ-w curve is well known. The σ-w curve can be reasonably approximated as a bilinear or even straight line. The main material parameters required to be determined are the fracture energy G_F, tensile strength f_t and Young's modulus E.

Fracture energy G_F was determined according the RILEM recommendation (1). The specimen size is shown in Fig 5.1. After a G_F test the beam was broken into two halves which were used for a three-point bending test and a tension test respectively.

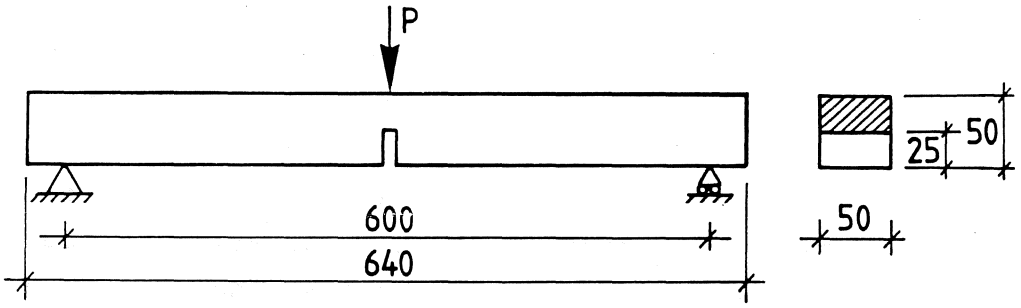

Fig 5.1 Specimen for fracture energy test

Tensile strength f_t was determined by use of the set-up by Petersson (36). Unnotched prism specimens with size 50*50*320 (mm) were used.

Dynamic Young's modulus E was determined by means of the resonance frequency method (41). The specimen size is 40*40*160 mm.

The characteristic length l_{ch} was calculated according to the formula:

$$l_{ch}=EG_F/f_t^2.$$

When the shape of the σ-w curve is not known, a stable direct tension test has to be performed to determine the σ-w curve. Tests for the σ-w curve determination were carried out by use of a testing set-up by Hassanzadeh, which is expected to diminish rotational instability. All-around notched prisms were used (Fig 5.2)

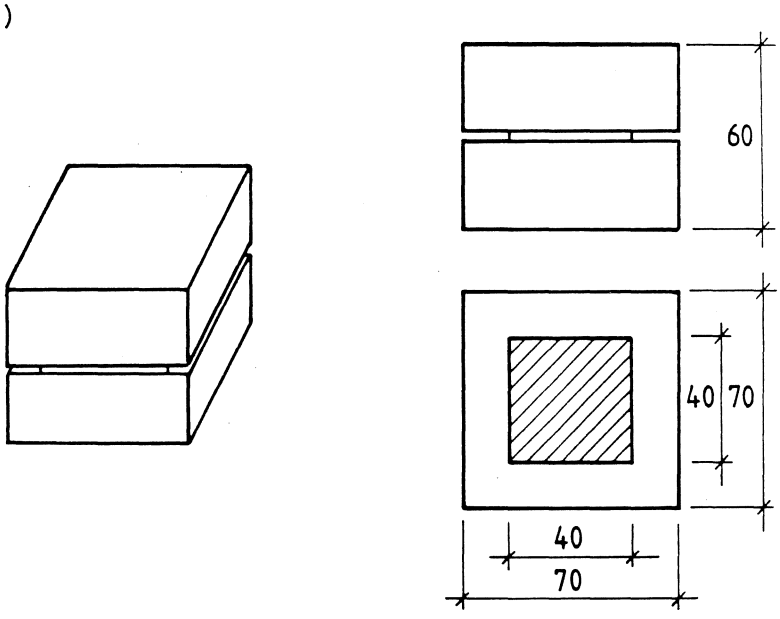

Fig 5.2 Specimen for σ-w curve test

(2) Investigation of structural behaviour

Three-point bending (TPB) tests and crushing tests of frame were performed to investigate structural behaviour for various materials.

For a three-point bending test (Fig 5.3) the flexural strength can be determined from the maximum load P by

$$f_f = \frac{3PL}{2bd^2} \qquad (1)$$

where b,d and L are thickness, depth and span of the beam respectively.

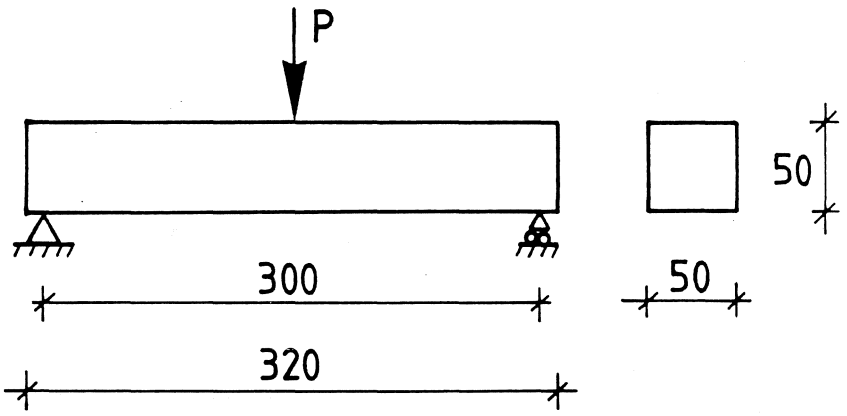

Fig 5.3 Specimen size for TPB test

For a frame test the load-deformation diagram was registered. The deformation was measured between the inner edges along the load line. The flexural strength can be approximately determined from the maximum load P according to beam theory by

$$f_f = \frac{3PD_1}{4bd^2}\left[2 - \frac{1}{1 + \frac{D}{D_1}\left(\frac{d}{d_1}\right)^3 \frac{1+d_0/d_1}{2(d_0/d_1)^2}}\right] \qquad (2)$$

where the notations are shown in Fig 5.4.

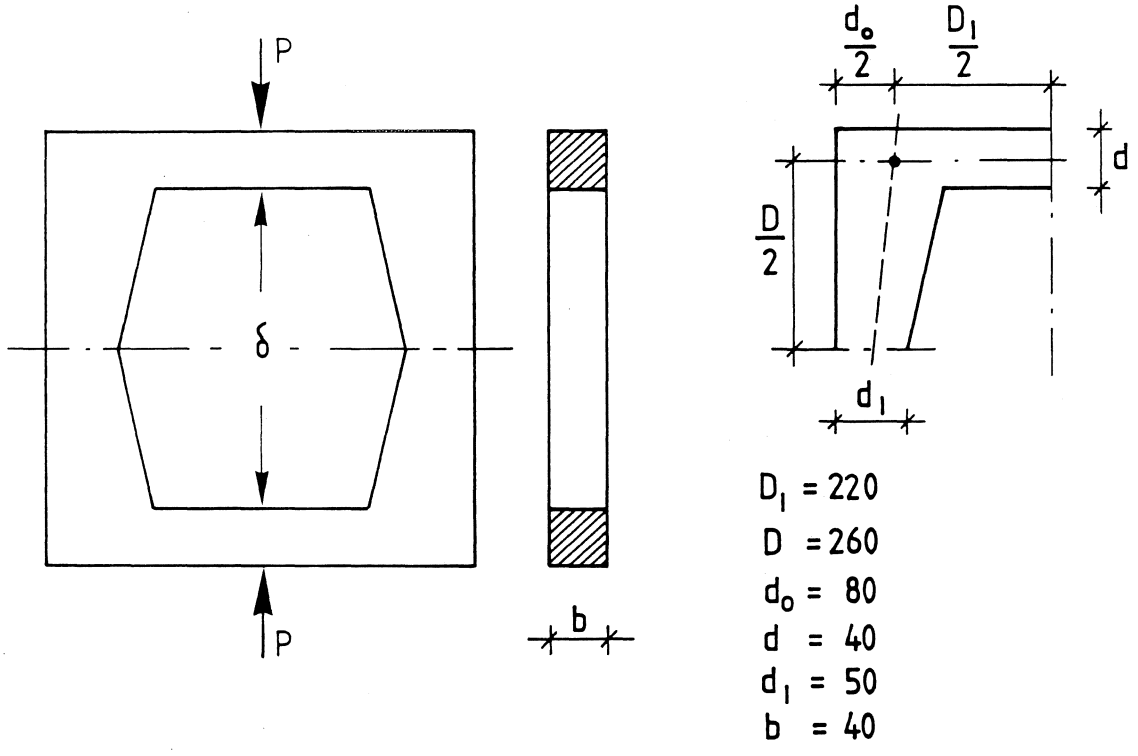

Fig 5.4 Specimen for frame test

5.2.2 Materials and preparation of specimens

(1) Materials

The tests were made in order to investigate the influence of fracture parameters on structural behaviour. Various materials from brittle to tough, cement mortar, lightweight concrete, fibre concrete and polymer concrete etc., were chosen in the tests. The test series is not finished yet, therefore only one part of tests are presented here.

Ordinary Portland cement and natural aggregate with modulus of fineness 1.82 were used. Krenit fibre, a synthetic fibre of polypropylene type, and RK carbon fibre, manufactured from polyacrylonitrile precursors, were chosen. The fibre properties are shown in Table 1.

The mix proportions and other data of materials used in tests are illustrated in Table 2.

(2) Preparation of specimens

For each test 3 large beams (50*50*640 mm), 3 small beams (40*40*160 mm) and 3 frames (see Fig 5.4) were cast. 3 around-notched prisms (see Fig 5.2) were also prepared when necessary. The specimens were covered in plastic at first 24 hours, then removed from the molds and stored in lime saturated water (+20°C) until testing. A 25 mm deep notch was introduced for each large beam by use of a diamond saw one day before testing.

Table 1 Fibre properties

Fibre type	Tensile strength (GPa)	Tensile modulus (GPa)	Ultimate elongation (%)	Density (g/cm^3)
Krenit	0.6	9-18	5-8	0.91
RK Carbon	2.5	215-240	1.05-1.40	1.78

Table 2 Materials and mixtures

Material	Cement:water :sand (Kg/m^3)	Max aggregate size d_{max} (mm)	Fibre content (vol %)	Fibre length (mm)	Testing age (day)
Mortar C1	440:220:1600	4			7
Mortar C2	480:240:1500	2			7
Carbon fibre concrete CC	700:350:1070	4	1	7	7
Krenit fibre concrete KC	600:300:1290	4	1	12	7

5.3 Experimental results and FCM analysis

5.3.1 Material parameters

The result of material parameters is given in Table 3. A low content of short carbon fibre with high modulus gives rise to increase in both tensile strength and fracture energy, although the charateristic length does not change so notably. The shape of the σ-w curve is similar to plain concrete and the σ-w curve is approximated as a bilinear one (Fig 5.5). As for the long krenit fibre with low moduli the fracture energy increases several times although the tensile strength hardly changes. The σ-w curve is simplified as a bilinear one in Fig 5.6.

Table 3 Material parameters

Material	G_F (Nm/m^2)	f_t (MPa)	E (GPa)	l_{ch} (m)
C1	59	2.8	33	0.25
C2	59	3.3	32	0.16
CC	153	4.4	29	0.23
KC	3440	3.2	27	9.07

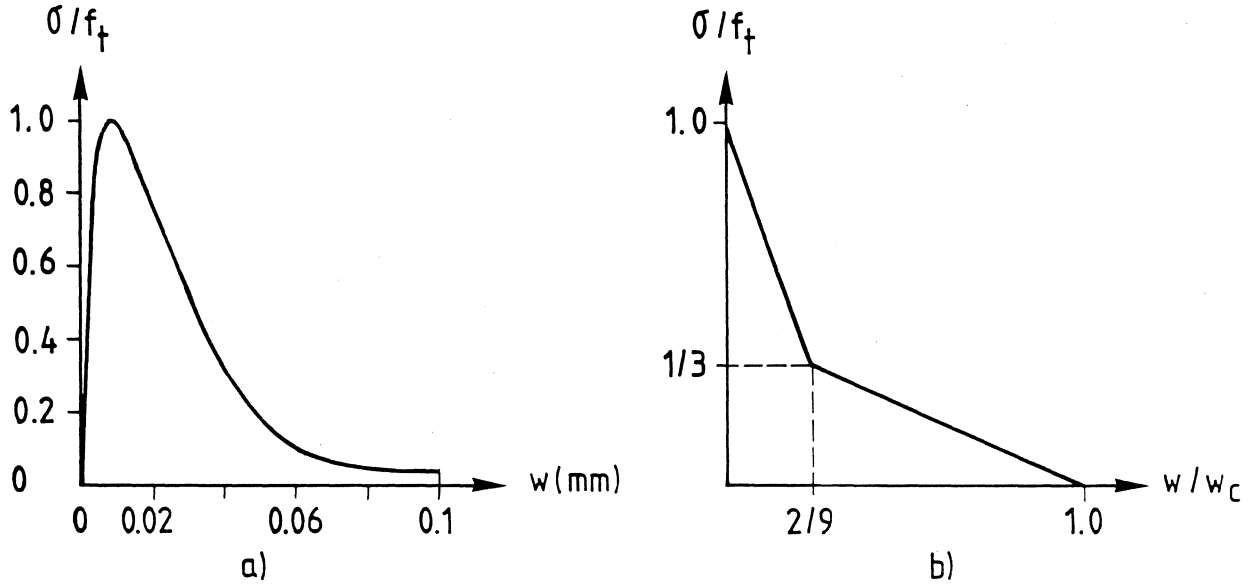

Fig 5.5 σ-w curve for carbon fibre concrete

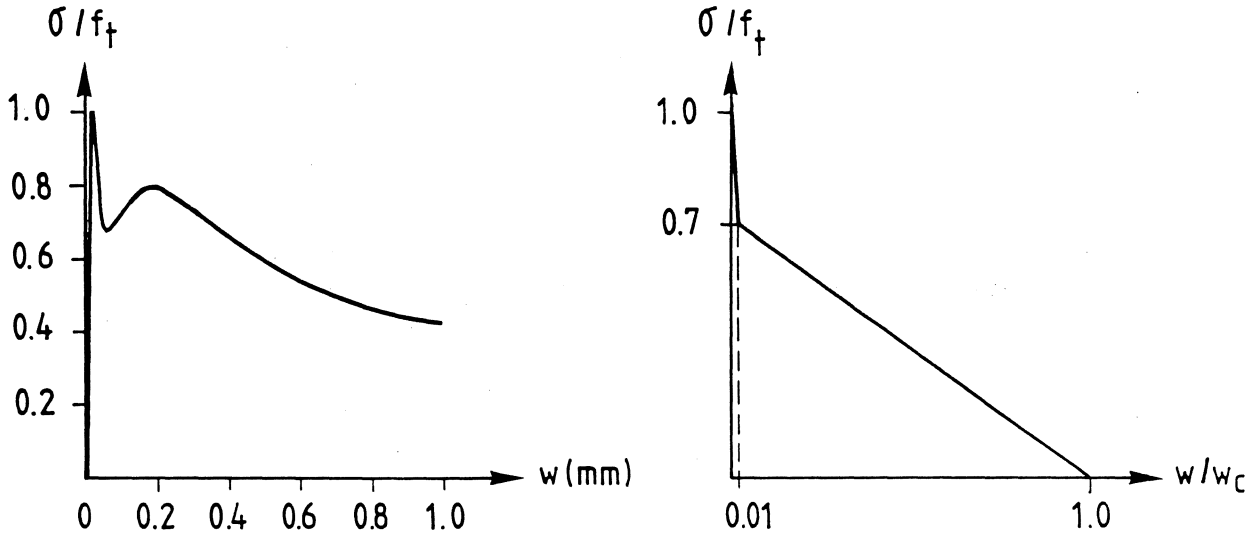

Fig 5.6 σ-w curve for krenit fibre concrete

5.3.2 FCM analysis and comparisons

(1) Numerical calculations

In the FEM analysis of frame test 8-node isoparametric elements were used. The element mesh was chosen as in Fig 5.7.

The flexural strength calculated according to the equation (2) is about 0.92 of the flexural strength obtained from the numerical calculation for the specimen size in Fig 5.3.

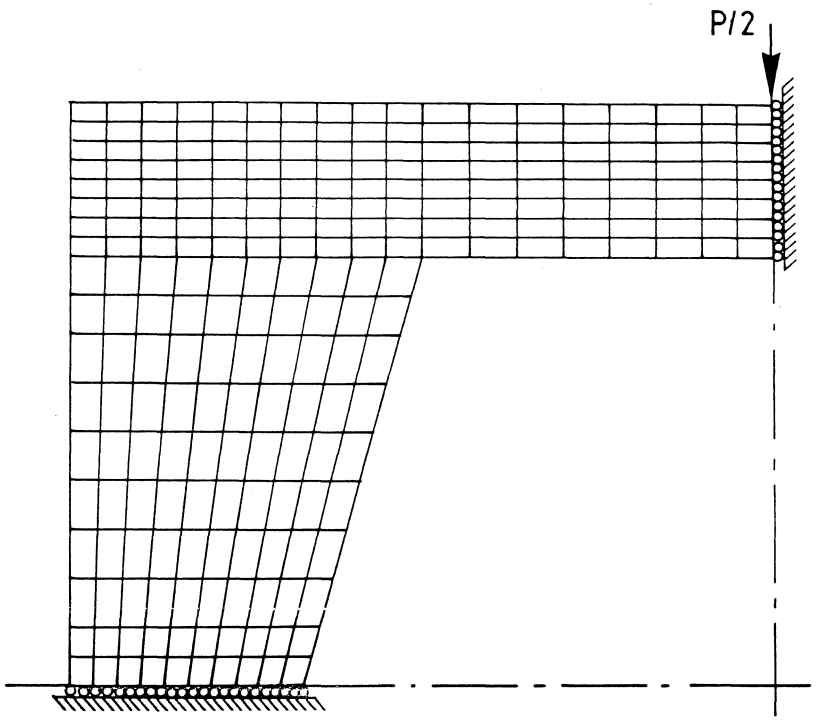

Fig 5.7 Element mesh for FEM analysis of frame test

(2) Simulation of frame test

Fig 5.8 shows the simulating load-displacement curves for different values of d/l_{ch}. Interaction of two cracks can be clearly seen from the structural response as d/l_{ch} changes.

In Fig 5.9 a comparison between the experimental and theoretical curves is made. The linear σ-w curve yields a better agreement with the experimental curve for material C2 than the bilinear one. Possibly a bilinear σ-w curve with a smaller initial slope may give a better approximation.

Fig 5.10 illustrates the experimental and simulating curves for a tough material, krenit fibre concrete. The theoretical prediction agrees in principle with the experimental curve. The material yields a highly plastic behaviour. For a tough material plasticity theory seems ready to be applicable.

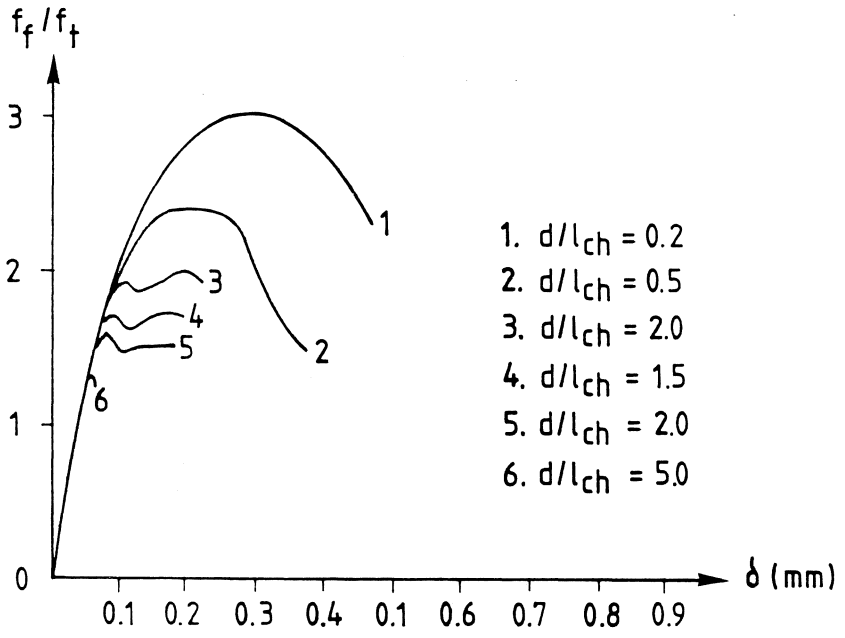

Fig 5.8 Simulation of frame test

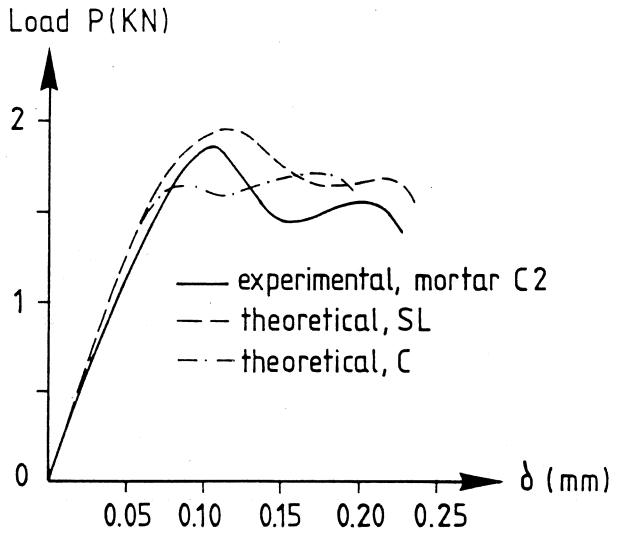

Fig 5.9 Experimental and theoretical responses of frame test for mortar C2

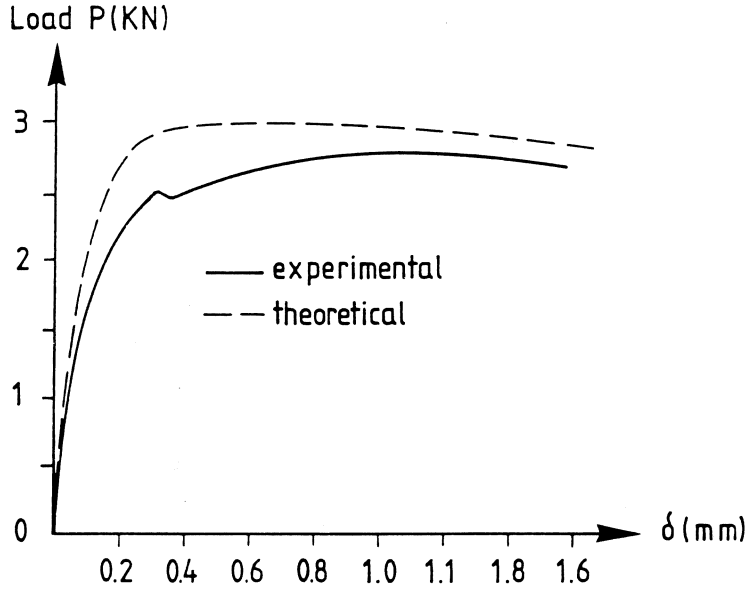

Fig 5.10 Experimental and theoretical responses of frame test for Krenit fibre concrete KC

(3) Strength analysis

Table 4 lists the experimental results and theoretical predictions of ratio between the flexural strength and tensile strength for both beam and frame tests. A reasonable agreement has been obtained. Comparisons are made in Fig 5.11 and Fig 5.12 respectively.

For the Krenit fibre concrete with remarkable plastic behaviour the flexural strength may be predicted by means of the ideal plasticity. In the σ-w curve (Fig 5.6) the tensile strength decreases to $0.7*f_t$ and keeps almost constant as w increases, thus the yield strength can be taken as $0.7*f_t$. Suppose that

Table 4 Experimental results and theoretical predictions of flexural strength

	TPB test			Frame test		
Material	d/l_{ch}	f_f/f_t theoretical	f_f/f_t experimental	d/l_{ch}	f_f/f_t theoretical	f_f/f_t experimental
C1	0.20	1.81	1.86	0.16	2.20	2.05
C2	0.31	1.69	1.79	0.25	1.93	2.01
CC	0.22	1.67	1.70	0.17	1.86	1.90
KC	0.0055	2.20	2.00	0.0044	3.02	2.78

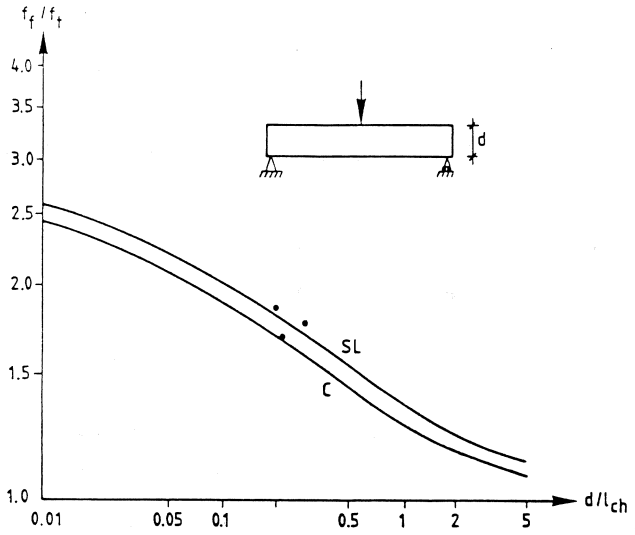

Fig 5.11 Theoretical and experimental variation of flexural strength in TPB tests

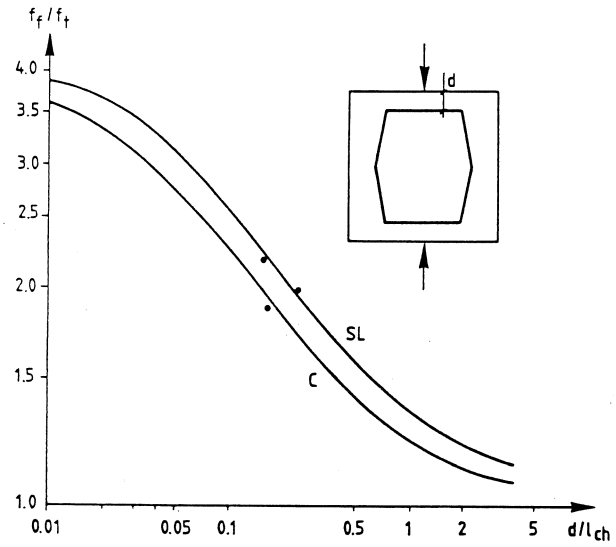

Fig 5.12 Theoretical and experimental variation of flexural strength in frame tests

compressive stresses can be infinitely great in the compressive edge and f_f/f_t for the TPB test is 2.1 and f_f/f_t for the frame test is 2.92, according to the ideal plasticity theory. They seem to agree with the experimental results.

6 CONCLUDING REMARKS

This report deals with stability and validity analyses of direct tension tests, and some investigation into structural behaviour of various materials in tensile fracture. One of the primary objectives is to study the influence of rotation in the damage zone on the stress-deformation curve. Another one is to further gain some insight into the general applicability of the Fictitious Crack Model.

Rotation in damage zones in tension tests can impose remarkable influence on the σ-w curve. A large tensile strength loss and highly distorted σ-w curve can result. The use of notched prisms does not seem to cause large errors.

The rotation stiffness of the testing set-up and specimen should be sufficient to counter-act possible rotations in damage zones in order to obtain a stable and reliable tension test. The prediction by the stability criterion agrees with the numerical results.

The bump effect, i.e. steep stress drops in the σ-w curve, has not been observed when rotation in damage zone is totally free or completely prevented. The effect is notable when rotation stiffness of the testing set-up is intermediately high. The bump effect seems to be directly related to the transition from a tension-bending to pure tension in the damage zone.

A number of tests, with both statically determinate and indeterminate specimens i.e a beam and a frame, are performed to investigate tensile fracture behaviour of various materials, from brittle to tough. For the statically indeterminate specimen the structural behaviour is more sensitive to the characteristic

length (l_{ch}) than for the statically determinate one. Compared to the experimental results, the FCM model seems to yield proper predictions.

A.1 REFERENCES

(1) 50 FMC Draft Recommendation (1985), "Determination of the Fracture Energy of Mortar and Concrete by Means of Three-point Bending Tests on Notched Beams", RILEM, Materiaux et Constructions, Vol. 18, No. 106, pp. 287-290.

(2) Bathe,K.J. (1982), Finite Element Procedures in Engineering Analysis, Englewood Cliffs, Prentice-Hall.

(3) Bazant, Z.P. and Oh, B.H. (1983), "Crack Band Theory for Fracture of Concrete", RILEM, Materiaux et Constructions, Vol. 16, No. 33, pp. 155-177.

(4) Bazant,Z.P. (1984), "Size Effect in Blunt Fracture: Concrete, Rock, Metal", J. Engrg. Mech., Vol. 110, No. 4, pp. 518-535.

(5) Bazant, Z.P. (1986), "Mechanics of Distributed Cracking", App. Mech. Rev., Vol. 39, No. 5, pp. 675-705.

(6) Bergan,P.G. (1973), "A Comparative Study of Different Numerical Solution Techniques as Applied to a Nonlinear Structural Problem", Computer Methods in Applied Mechanics and Engineering, No. 2, pp. 185-201.

(7) Carpinteri, A., Di Tommaso, A. and Fanelli, M. (1985), "Influence of Material Parameters and Geometry on Cohesive Crack Propagation", Fracture Mechanics of Concrete, Ed F.H. Wittmann, Lausanne.

(8) Carpinteri, A. (1986), "Limit Analysis for Elastic-softening Structures: Scale and Slenderness Influence on Global Britt-

leness", Brittle Matrix Composites, Ed A.M. Brandt and I.H. Marshall, Elsvier Applied Science Publishers LTD, England.

(9) Cedolin,L., Dei Poli,S. and Iori,I. (1987), "Tensile Behavior of Concrete", J. Engrg. Mech., ASCE, Vol. 113, No. 3, pp. 431-449.

(10) Chen, W.F. (1982), Plasticity in Reinforced Concrete, McGraw-Hill Book Company, USA.

(11) Clarin, P.G. (1987), "Fracture Analysis of Center Cracked Infinite Plates of Linear Softening", Engrg. Frac. Mech., Vol. 27, No. 2, pp. 231-245.

(12) Cook, R.D. (1981), Concepts and Applications of Finite Element Analysis, Second edition, John Wiley Sons, Inc., Canada.

(13) Craig, R.J., Decke, J., Dombrowski, L., Laurencelle,R. and Federovich, J. (1987), "Inelastic Behavior of Reinforced Fibrous Concrete", J. Struct. Engrg., ASCE, Vol. 113, No. 4, pp. 803-817.

(14) Gopalaratnam, V.S. and Shah S.P. (1985), "Softening Response of Plain Concrete in Direct Tension", ACI Journal, pp. 310-323.

(15) Gustafsson, P.J. and Hillerborg, A. (1984), "Improvements in Concrete Design Achieved through the Application of Fracture Mechanics", Application of Fracture Mechanics to Cementitious Composites, Ed S.P. Shah, Northwestern Univ, USA.

(16) Gustafsson, P.J. (1985), "Fracture Mechanics Studies of Non-yielding Materials Like Concrete: Modelling of Tensile

Fracture and Applied Strength Analyses", Report TVBM-1007, thesis, Div. of Building Material, Univ. of Lund, Sweden.

(17) Gylltoft, K. (1983), "Fracture Mechanics Models for Fatigue in Concrete Structures", Doctoral Thesis 1983:25D, Div. of Struct. Engrg., Luleå Univ. of Tech., Sweden.

(18) Hassanzadeh, M., Hillerborg, A. and Zhou, F.P. (1987), "Tests of Material Properties in Mixed Mode I and II", Fracture of Concrete and Rock, Ed. S.P. Shah and S.E. Swartz, pp. 353-358.

(19) Hillerborg, A., Modéer, M. and Petersson, P.E. (1976), "Analysis of Crack Formation and Crack Growth in Concrete by means of Fracture Mechanics and Finite Elements", Cem. Concr. Res., Vol. 6, pp. 773-782.

(20) Hillerborg, A. (1978), "A Model for fracture Analysis", Report TVBM-3005, Div. of Building Materials, Univ. of Lund, Sweden.

(21) Hillerborg, A. (1985), "Numerical Methods to Simulate Softening and Fracture of Concrete", Application of Fracture Mechanics to Concrete Structures, Vol. 2, Eds. Carpinteri etc., Martin Nijhoff Publishers.

(22) Hillerborg, A. (1985), "Influence of Beam Size on Concrete Fracture Energy Determined According to a Draft RILEM Recommendation", Report TVBM-3021, Div. of Building Materials, Univ. of Lund, Sweden.

(23) Hillerborg, A. (1985), "Determination and Significance of the Fracture Toughness of Steel Fibre Concrete", Steel Fibre Concrete, Ed. S.P. Shah and Å. Skarendahl, Swedish Cement and

Concrete Research Institute, Stockholm, pp. 257-271.

(24) Hillerborg, A. (1988), "Applications of Fracture Mechanics to Concrete", Report TVBM-3030, Div. of Building Materials, Univ. of Lund, Sweden.

(25) Hillerborg, A. (1988), "Mixed Mode Fracture in Concrete", to appear on the Seventh International Conference on Fracture, 1989, Houston, USA.

(26) Hordijk, D.A., Reinhardt, H.W. and Cornelissen, H.A.W. (1987), "Fracture Mechanics Parameters of Concrete from Uniaxial Tensile Tests as Influenced by Specimen Length", Fracture of Concrete and Rock, Ed. S.P. Shah and S.E. Swartz, USA, pp. 138-149

(27) Jayatilaka, A. de S. (1979), Fracture of Engineering Brittle Materials, Applied Science Publishers LTD, England.

(28) Kaplan, M.F. (1961), "Crack Propagation and the Fracture of Concrete", ACI Journal, Vol. 58, pp. 591-610.

(29) Labuz, J.F. (1985), "A Study of the Fracture Process Zone in Rock", PhD dissertation, Northwestern Univ,Evanston,Illinois.

(30) Modéer, M. (1979), "A Fracture Mechanics Approach to Failure Analysis of Concrete Materials",Report TVBM-1001, thesis, Div. of Building Materials, Univ. of Lund, Sweden.

(31) Nallathambi, P. and Karihalloo, B.L. (1986), "Prediction of Load-deflection Behavior of Plain Concrete from Fracture Energy", Cem. Concr. Res., Vol. 16, pp. 373-382.

APPENDIX 1

(32) Ngo, D. and Scordelis, A.C. (1967), "Finite Element Analysis of Reinforced Concrete Beams", J. Am. Concr. Inst., Vol. 64, No. 3, pp. 152-163.

(33) Oldenburg, M. (1985), "Finite Element Analysis of Tensile Fracture Structures", Licentiate Thesis 1985:010L, Div. of Computer Aided Analysis and Design, Luleå Univ., Sweden.

(34) Petersson, P.E. (1980), "Fracture Energy of Concrete: Method of Determination", Cem. Concr. Res., Vol. 10, pp. 78-79.

(35) Petersson, P.E. (1980), "Fracture Energy of Concrete: Practical Performance and Experimental Results", Cem. Concr. Res., Vol. 10, pp. 91-101.

(36) Petersson, P.E. (1981), "Direct Tensile Tests on Prismatic Concrete Specimens", Cem. Concr. Res., Vol. 11, pp. 51-56.

(37) Petersson, P.E. (1981), "Crack Growth and Development of Fracture Zones in Plain Concrete and Similar Materials", Report TVBM-1006, thesis, Div. of Building Material, Univ. of Lund, Sweden.

(38) Rots, J.G., Nauta, P., Kusters, G.M.A. and Blaauwendraad, J. (1985), "Smeared Crack Approach and Fracture Localization in Concrete", Heron, Vol. 30, No. 1, Delft Univ. of Tech. and Inst. TNO for Build. Mat. and Struct., The Netherlands.

(39) Rots, J.G. (1988), "Computational Modeling of Concrete Fracture", Thesis, Dept. of Civil Engrg., Delft Univ. of Tech., The Netherlands.

REFERENCES

(40) Van Mier, J.G.M. (1986), "Fracture of Concrete under Complex Stress", Heron, Vol. 31, No. 3, Delft Univ. of Tech. and Inst. TNO for Build. Mat. and Struct., The Netherlands.

(41) Vinkeloe, R. (1962), "Prüfverfahren Zurermittlung des Dynamischen Elastizitätsmodulus von Betonprismen", Tonindustrie Zeitung , Vol. 86, pp. 272-276.

A.2 NOTATIONS

Notations and symbols are explained in the text when they first occur. The main notations are listed as below:

Latin letters

a	notch depth
e	eccentricity
E	Young's Modulus
f_f	flexural strength
f_t	tensile strength
G_c	critical energy release rate
G_F	fracture energy
I	moment of inertia
K_c	fracture toughness
K_r	rotation stiffness of testing machine
K_t	tension stiffness of testing machine
L	length
l_{ch}	$=EG_F/f_t^2$, characteristic length of material
M	moment, or mass
P	load, force
w	deformation of damage zone
w_c	maximum deformation of damage zone

Greek letters

δ	deflection, deformation
ϵ	strain
θ	rotation angle
μ	micro, 10^{-6}
σ	stress
σ_y	yield strength